Session A

A-17-M

Solar Cells Based on p-n Junction Embedded Single-Walled Carbon Nanotubes

S. Kodama*, Y. F. Li, T. Kaneko and R. Hatakeyama
Department of Electronic Engineering, Tohoku University, Sendai 980-8579, Japan
*kodama@plasma.ecei.tohoku.ac.jp

Single-walled carbon nanotubes (SWNTs) have many advantages in making solar cells, such as large surface areas, enormous current carrying capability, high mechanical strength and chemical stability. In addition, we can change their band gap energy by tuning the diameter and their semiconducting properties by encapsulating foreign materials[1]. This characteristic makes it possible to absorb sun light in the infrared region.[2]

The p-n junction in SWNTs is made by partially encapsulating foreign materials which work as electron donors, such as potassium (K). The K encapsulated SWNTs (K@SWNTs) are used for solar cell fabrication. Figure 1 shows the structure of field-effect transistor (FET) by using K@SWNT. The FET devices exhibit rectifying behaviors, suggesting that SWNTs contain p-n junctions inside. In particular, we have succeeded in observing a down shift of *I-V* characteristics under infrared light (1550 nm and 1650 nm) irradiation, as seen in Fig. 2. These results show that the photovoltaic effect appears in the case of using p-n junction embedded SWNTs and prove the potentials of SWNTs for infrared solar cell applications.

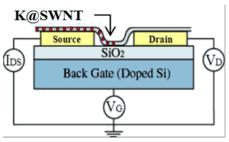

Fig. 1. Schematic of FET using individual K@SWNT.

Our results indicate that it is possible to make the high efficiency (up to $\eta = 23\%$) infrared solar cell based on p-n junction embedded SWNTs by encapsulation of the foreign atoms or molecules.

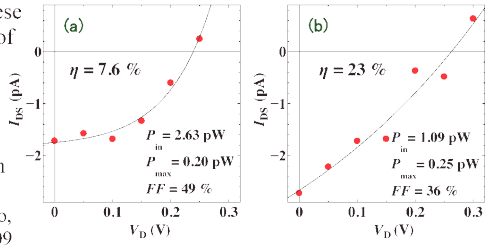

Fig. 2. *I-V* characteristics of K@SWNT-FET under (a) 1550 nm and (b) 1650 nm light illumination. $V_G = 0$ V

Reference : 1) R. Hatakeyama, T. Kaneko, W. Oohara, Y. F. Li, T. Kato, K Baba, and J Shishido: *Plasma Sources Sci. Technol.*, 17, 024009 (2008), 2) R. Hatakeyama, Y. F. Li, T. Y. Kato, and T. Kaneko, *Appl. Phys. Lett.*, 97, 013104 (2010).

A-P04-G

Pulsed Laser Deposition of Alq_3 Thin Films Using Target Cooling by Liquid Nitrogen

T. Ohshima*, A. Kawashima, H. Kawasaki, Y. Suda and Y. Yagyu
Sasebo National College of Technology, 1-1 Okishin, Sasebo, Nagasaki 857-1193, Japan, *ohshima@sasebo.ac.jp

We used pulsed laser deposition (PLD) to prepare aluminum tris-8-hydroxyquinoline (Alq_3) thin films as a typical luminescent layer of organic electroluminescence (OEL) devices. Many deposition parameters of PLD such as laser fluence, ambient gas and pressure, target-to-substrate distance, and substrate temperature influence of film growth. However, effect of target temperature has never been investigated. The target temperature increases after film deposition by laser irradiation. In order to keep the target temperature during film deposition we used liquid nitrogen. In this study, the effect of target temperature in PLD on characteristics of Alq_3 thin films was investigated.

We prepared Alq_3 thin films at different target temperatures of –120ºC (liquid nitrogen) and room temperature (RT). These films were also deposited on room-temperature substrates in vacuum using laser fluence of 1.5 J/cm^2. Figure 1 shows XPS spectra of Alq_3 thin films deposited on Si substrate by cooling target and room-temperature target. Peak energy of the Al 2p, C 1s, N 1s, and O 1s peaks shifted toward lower binding energy than that of RT. Al 2p and N 1s peaks show that Alq_3 thin films deposited by cooling target have the structure such as Al-O-C and N in Alq_3[1].

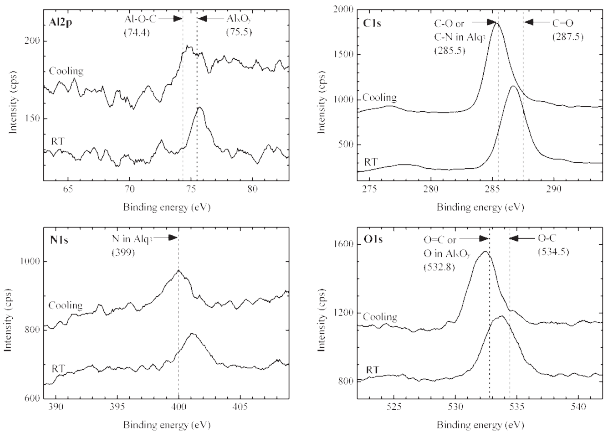

Fig. 1. XPS spectra of Alq_3 thin films deposited by cooling target and room-temperature target.

1) T.P. Nguyen, J. Ip, P. Jolinat and P. Destruel, *Applied Surface Science*, 172, 75-83 (2001).

Session B

B-P07-G

Diamonds Utilized in the Development of Single Ion Detector with High Spatial Resolution

S. Onoda*, T. Yamamoto, T. Ohshima, J. Isoya[1)], T. Teraji[2)] and K. Watanabe[2)]
Japan Atomic Energy Agency (JAEA), Gunma, Japan, [1)] University of Tsukuba, Tsukuba, Japan, [2)] National Institute for Materials Science (NIMS), Tsukuba, Japan, *onoda.shinobu@jaea.go.jp, yamamoto.takashi@jaea.go.jp, ohshima.takeshi20@jaea.go.jp, isoya.junichi.fw@u.tsukuba.ac.jp, teraji.tokuyuki@nims.go.jp, watanabe.kenji.aml@nims.go.jp

We are developing the single ion detection system with high spatial resolution. By capturing the ion induced luminescence from a phosphor by using Charge Coupled Device (CCD) Camera, the location where ion hit is observed. In this study, a single crystal diamond is used as a phosphor. The measurement system contains a beam extraction window (Kapton film) under the mirror, the diamond on micro XYZ stage, and a photon detection equipments including the microscope (Olympus, BX51M), the image intensifier (Hamamatsu, C8600), and cooled CCD Camera (Hamamatsu, C4880-50-26A). Ion beams accelerated by the AVF Cyclotron are extracted from vacuum to air via the Kapton film. Extracted ions penetrate the diamond. The photons from the diamond are detected by the cooled CCD camera. The inset of Fig. 1 shows the image of cooled CCD camera when 150 MeV Argon ions penetrate the diamonds. Three spots are detected and each spot can be distinguished. The Full Width at Half Maximum (FWHM) of spot is about 4 μm. The position where ion hits the sample can be calculated from the center of mass of each spot. Branson et al., reported that YAG:Ce is the most promising materials as a phosphor[1,2)]. Fig. 1 shows the normalized spectrum of intensity observed from ZnS, YAG:Ce and diamond. We found that the diamond is comparable to YAG:Ce from the point of view of spatial resolution because of the same spot size. Although not shown here, the intensity of luminescence from diamond is slightly higher than that from YAG:Ce. According to these results, we suggest that both diamond and YAG:Ce are suitable for single ion detection with high spatial resolution.

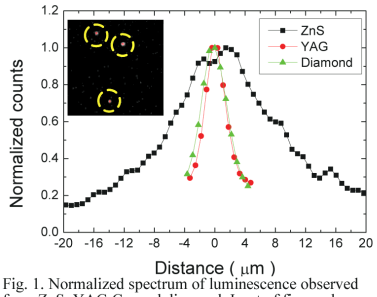

Fig. 1. Normalized spectrum of luminescence observed from ZnS, YAG:Ce, and diamond. Inset of figure shows the CCD image when 150 MeV Ar ions strike diamond. Three spots are found in the dashed circles.

References:1) J. V. Branson et al, *Nucl. Instr. Meth. B*, in press. 2)J. V. Branson et al, *Nucl. Instr. Meth. B*, 267, 2085-2089 (2009)
Acknowledgements: This work was partly supported by the Strategic Japanese-German Joint Research Program in 2009 from the Japan Science and Technology Agency.

B-P06-M

Biocompatible Evaluation of PTFE Fiber

S. Morisaki*[1)], A. Ogura[1)], S. Hamago[2)], T. Tanaka[3)], K. Mizutani[3)], A. Yamada[3)], and Y. Suzuki[1), 3)]
[1)] Meiji University, 1-1-1 Higashimita, Tama-ku, Kawasaki-shi, Kanagawa 214-8571, Japan, [2)] Tokyo University of Science, 1-3 Kagurazaka, Shinjuku-ku, Tokyo 162-8601, Japan, [3)] RIKEN 2-1 Hirosawa, Wako-shi, Saitama 251-0198, Japan, *smorisaki@riken.jp

Polytetrafuluoroethylene (PTFE) fiber is one of the medical materials used for brain surgery and cardiovascular surgery such as reinforcement of the suture part and prosthesis of the defect part after the excision. However, there are many problems due to its poor adhesion to fibrin glue and tissue. This study concerned fabrication of novel cell adhesive materials by ion beam irradiation. PTFE fiber was irradiated with 150 keV-Kr^+ beams at fluences of 1×10^{14}, 5×10^{14}, and 1×10^{15} ions/cm^2. In vitro L929 mouse fibroblast cells were cultured on non-irradiated and ion-irradiated specimen and adhesion of fibrin glue were also evaluated. Surface characterization was performed using SEM, contact angle, XPS, and Raman spectroscopy. Japanese white rabbits were used in this in vivo animal study. The specimens were removed from the body at four weeks after implantation.

Cell attachment to the ion-irradiated fiber dramatically improved as compared with non-irradiated. PTFE fiber irradiated with 150 keV-Kr^+ beam at a fluence of 5×10^{14} ions/cm^2 showed best cell adhesive property. Raman spectroscopic study revealed the peak which included D band and G band was confirmed. This result means the fiber surface was carbonized by ion-beam irradiation. The carbonization was also revealed from C_{1s} spectra obtained by XPS study. It was thought amorphous carbon induced by ion beam irradiation was major factor for improving cell invasion. Animal study indicated cells extended inside in Kr^+-irradiated PTFE fiber, however, cells do not extend inside in case of non-irradiated PTFE fiber (Fig. 1). It is therefore very likely that ion-implanted PTFE fiber will be applicable for clinical use.

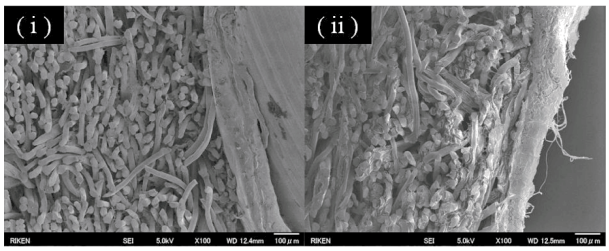

Fig. 1. SEM micrograph of (i) non-irradiated and (ii) Kr^+-irradiated PTFE fiber in vivo study.

Session C

C-02-G

Characterization of Morphology and Chemical Composition of Inclusion in Steel using Small-Angle X-ray and Neutron Scattering

Y. Oba*, S. Koppoju, M. Ohnuma, Y. Kinjo[1], S. Morooka[2], Y. Tomota[1], J. Suzuki[3], D. Yamaguchi[4], S. Koizumi[4], M. Sato[5], T. Shiraga[6]

National Institute for Materials Science, Tsukuba, Ibaraki 305-004, [1]Ibaraki University, Hitachi, Ibaraki 316-8511, [2] Yokohama National University, Yokohama, Kanagawa, [3] Comprehensive Research Organization for Science and Society, Tokai Ibaraki 319-1106, [4] Japan Atomic Energy Agency, Tokai Ibaraki 319-1195, [5] Japan Synchrotron Radiation Research Institute, Sayo-cho, Hyogo 679-5198, [6] JFE Bars & Shapes Corporation, Sendai, Miyagi 983-0001 *OBA.Yojiro@nims.go.jp

Since inclusion strongly affects the properties of steels, the characterization and control of its morphology is important. For free cutting steels, inclusion is used to obtain high machinability. To improve the machinability, the quantitative analysis of the morphology is a key issue. For such quantitative characterization of the microstructures, small-angle X-ray (SAXS) and neutron scattering (SANS) are suitable because they provide the representative values averaged in significantly large area. In addition, combined use of SAXS and SANS enables us to precisely analyze the chemical composition of the microstructures even embedded in matrices. In this study, we present the characterization of the inclusion in the free cutting steel using SAXS and SANS.

The SAXS measurements were performed using the laboratory SAXS instruments with Mo and Cr targets. For the microstructures larger than several hundreds nanometers, ultra-small-angle scattering (USAXS and USANS) techniques are required. For the USAXS measurements, a 2D USAXS instrument at BL19B2 in SPring-8 was used. The USANS and SANS measurements were performed using the PNO and the SANS-J-II in JAEA.

Figure 1 (a) shows the 2D USAXS pattern of the free cutting steel. The pattern includes an anisotropic component elongated perpendicular to the rolling direction (RD) and an isotropic component. The experimental pattern can be explained by the simulated model composed of elongated ellipsoidal and spherical particles (Fig. 1(b)). The ratio of the SAXS and SANS profiles indicates that the chemical compositions of the inclusions are manganese sulfide.

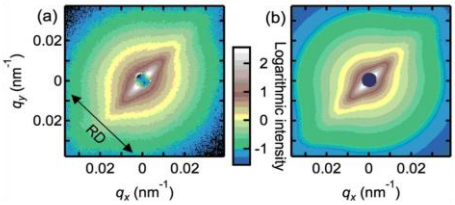

Fig. 1. 2D USAXS patterns: (a) experimental result and (b) simulated pattern composed of elongated ellipsoidal and spherical inclusions.

Session D

D-P25-G

Enhancement of Intragrain Critical Current Density in Bi-based Superconductor

H. Tanaka*, H. Yoshikawa[1], C. Tsuruta[2], Y. Matsui[2], and S. Kishida[3]

Yonago National College of Technology, Tottori 683-8502, Japan, [1] National Institute for Materials Science, Hyogo 679-5148, Japan, [2] National Institute for Materials Science, Tsukuba 305-0044, Japan, [3] Tottori University, Tottori 680-8552, Japan, *hitanaka@yonago-k.ac.jp

We grew Bi-based superconducting whiskers with various substitution ratios of Ca^{2+} ions for Sr^{2-} sites (:Ca/Sr substitution ratios) by an Al_2O_3-seeded glassy quenched platelet method.

We found that the critical current density (J_c) of the Bi-based superconducting whiskers is widely controllable by just changing Ca/Sr substitution ratios. As shown in Fig. 1, the J_c increases by a factor of 200. The Bi-based superconducting whisker with the Ca/Sr substitution ratio of about 25 % shows a high J_c of 2×10^5A/cm^2 at 40 K in self-field[1].

From the analysis by X-ray photoemission spectroscopy using synchrotron radiation and high-resolution transmission electron microscopy, we found that the whisker has a strong pinning center. The pinning center consists of a structural distorted two-dimensional nanoplane defect which is introduced by controlling a strain in a Sr-O layer.

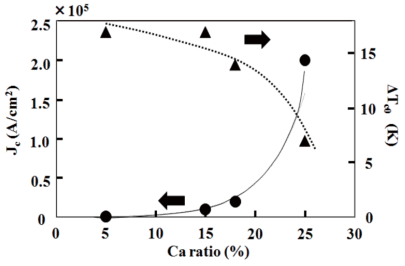

Fig. 1. Effect of Ca^{2+} substitution for Sr^{2+} sites on the whisker's J_c and degree of flux creep(ΔT_{c0}). The J_c is measured at 40 K in self-field. The ΔT_{c0} is measured in a field of 1T.

References: 1) H. Tanaka, H. Yoshikawa, S. Ueda, C. Tsuruta, Y. Matsui and S. Kishida, *J. Appl. Phys.*, (accepted).

D-18-G

High-Permittivity and Low-Loss $BaTiO_3$-Cu Composite Films Using Aerosol Deposition

Y. H. Kim and S. M. Nam*
Dept. of Electronic Materials Engineering, Kwangwoon University, 447-1, Wolgye-dong, Nowon-gu, Seoul 139-701, Korea
*smnam@kw.ac.kr

Recently, high-permittivity composites have been researched with the requirements of high capacity multilayer ceramic capacitors. To follow this trend, high-permittivity conductive filler-insulator composites, which are based on percolation theory, have attracted great attention. As for conductive filler-polymer composites, a high loss and the high frequency dependence of dielectric prosperities are main problems even though they show a high permittivity[1]. To overcome these limits and achieve a giant permittivity, $BaTiO_3$-metal bulk composites have been studied[2]. For a high capacitance, however, the thin and thick film process of ceramic-metal composites should be developed.

In this study, we have attempted the fabrication of $BaTiO_3$-Cu composite thick films by an aerosol deposition (AD) process[3], which is able to fabricate ceramic thin and thick films, with subsequent post-annealing to examine their potential as a fabrication process for low-loss ceramic-metal composite films with high ε_r. The ε_r and tanδ of as-fabricated $BaTiO_3$-Cu composite films with the Cu content of 10.2 vol.% were 328 and 0.028 at 100 kHz, respectively, as shown in Fig. 1. After a subsequent post-annealing at 400°C, the ε_r of the composite films was 515, which is 6 times larger than that of the as-fabricated $BaTiO_3$ films by AD, with a very low loss (tanδ = 0.019). Additionally, to confirm the causes leading to the high ε_r, ceramic-metal composite models were designed and their ε_r was calculated using the 3-dimentional electrostatic simulation.

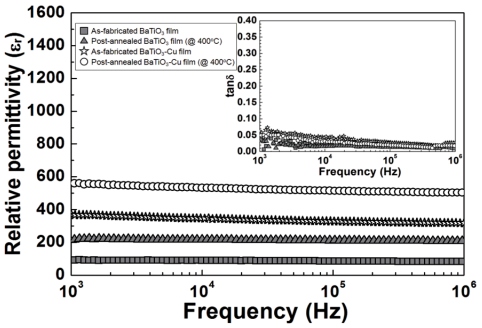

Fig. 1. Frequency dependence of the dielectric properties of the as-fabricated $BaTiO_3$ films and $BaTiO_3$-Cu composite films.

References : 1) M. Panda et al., *Appl. Phys. Lett.*, 92,132905-1-4 (2008), 2) C. Pecharroman et al., *Adv Mater.*, 13, 1541-4 (2001), 3) J. Akedo, *J. Therm. Spary Techn.*, 17, 181-98 (2008)

D-20-D

Metal-oxide core-shell nanowire structure for solar energy conversion

Miao Zhong*[1)], Yanbo Li[1)], Abel Sibai[2)], Georges Bremond[2)], Ichiro Yamada[1)] and Jean-Jacques Delaunay*[1)]
[1)]Department of Mechanical Engineering, The University of Tokyo, 7-3-1 Hongo, Bunkyo-ku, Tokyo 113-8656, Japan, [2)]Institut des Nanotechnologies de Lyon (INL-UMR5270), Universit´e de Lyon, CNRS, INSA, Lyon, B^atiment Blaise Pascal, 7 Avenue J Capelle, 69621 Villeurbanne Cedex, France
*jean@mech.t.u-tokyo.ac.jp, miaozhong@lelab.t.u-tokyo.ac.jp

A two-step chemical vapor deposition process is being developed to fabricate vertically aligned ZnO-$ZnGa_2O_4$ core-shell nanowires. In this process, the vertical alignment of the nanowires is achieved by the selection of the substrate and the deposition of metallic nanoparticles acting as catalysts for the nanowire growth. The process realizes an homogeneous deposition over large areas of core-shell nanowires and allows for the control of the density of the core-shell nanowires. The ZnO-$ZnGa_2O_4$ core-shell nanowires are electrically connected by their bases through a thick underlayer of the same material, thus realizing electrical contact of the array of nanowires. The microstructure of the core shell nanowires was analyzed by X-ray diffraction and transmission electron microscopy. The ZnO cores and $ZnGa_2O_4$ shells are of single crystal quality and have aligned crystallographic orientations. The ZnO cores grow along [0001] which is aligned with the [111] of the $ZnGa_2O_4$ shells. The optoelectronic properties are studied by diffuse reflectance, photoluminescence, and photocurrent. The two near-band-edge absorptions of ZnO and $ZnGa_2O_4$ are clearly observed confirming the core-shell structure. Further, characteristic photoluminescence peaks of the ZnO and $ZnGa_2O_4$ are observed. Finally, the dense array of vertically aligned ZnO-$ZnGa_2O_4$ core-shell nanowires shows a stable and promising photoelectric current. The fabricated structure consisting of vertically aligned core-shell nanowires electrically connected by their bases offers an advantageous structure to be used as a photoanode in photoelectrochemical cells for solar light harvesting and conversion into chemical energy in the form of hydrogen.

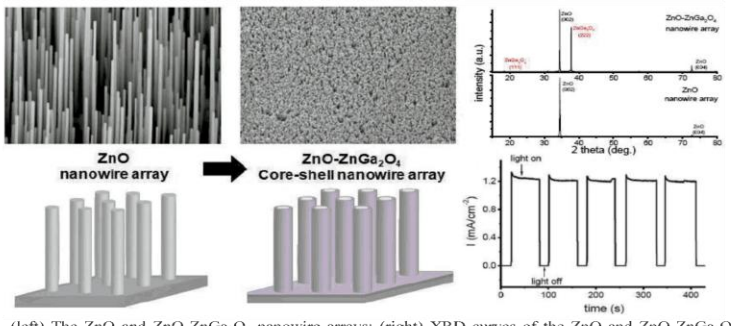

Fig. (left) The ZnO and ZnO-$ZnGa_2O_4$ nanowire arrays; (right) XRD curves of the ZnO and ZnO-$ZnGa_2O_4$ nanowire arrays and photocurrent curve of the ZnO-$ZnGa_2O_4$ nanowire array when used as a photoanod at a bias of 0.7 V vs. Ag/AgCl (right).

Session E

E-08-G

Influences of 90° Domain Walls upon Piezoelectric Properties of $Bi_4Ti_3O_{12}$ Single Crystals

Y. Kitanaka*, Y. Noguchi, and M. Miyayama
Research Center for Advanced Science and Technology, The University of Tokyo,
*y-peichun@crm.rcast.u-tokyo.ac.jp

$Bi_4Ti_3O_{12}$ (BiT), which belongs to the family of bismuth layer-structured ferroelectrics, has been regarded as a promising Pb-free material because of its large spontaneous polarization and high Curie temperature.[1,2] Despite its high potential as a ferroelectric/piezoelectric material, BiT often suffers from degraded polarization properties due to lattice defects such as oxygen vacancies.[3] Because the poor polarization properties as well as the difficulty in growing thick crystals have made the investigation of electrical properties difficult, few studies on piezoelectric properties of BiT have been reported to date. In this study, we have investigated the influence of domain structure upon the piezoelectric properties of high-quality BiT single crystals grown under high-oxygen-pressure (high-Po_2) atmosphere.

BiT single crystals with a relatively large thickness (> 3 mm) along the *c* axis were successfully obtained by a the top-seeded solution growth (TSSG) method under a Po_2 of 0.9 MPa.[4,5] The crystals obtained were annealed in air at 900 °C before the measurements of piezoelectric properties. Figure 1 shows well-established butterfly loops observed in the electric-field(E)-induced bipolar strain along <100> and <110> of the crystals. A piezoelectric strain constant (d^*) estimated by E-induced unipolar strain curves along <110> was a larger value of 56 pm/V than that along <100> (37 pm/V). By using the piezoelectric constants (d_{11}, d_{12} and d_{26}) evaluated from resonance-antiresonance characteristics of the BiT crystals, the value of E-induced piezoelectric strain along <110> was calculated to be 36 pm/V, which cannot explain the large d^* measured along <110>. Optical and piezoresponce force microscope observations revealed that 90° domains with a typical width of 10 μm were formed in the BiT crystals after applying an E along <110>. It is considered that the large d^* along <110> originates from a domain-wall effect due to the dense 90° domain structure.

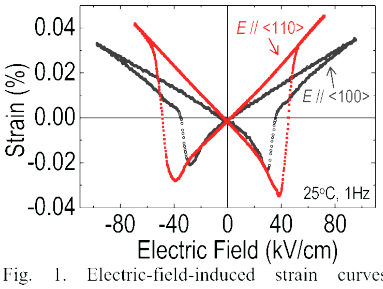

Fig. 1. Electric-field-induced strain curves measured along <100> and <110> of the BiT crystals grown by the high-oxygen-pressure TSSG method.

References: 1) S. E. Cummins and L. E. Cross: *J. Appl. Phys.* 39 (1968) 2268. 2) T. Takenaka and K. Sakata: *Ferroelectrics* 19 (1978) 172. 3) Y. Kitanaka *et al.*: *Phys. Rev. B* 81 (2010) 094114. 4) K. Yamamoto *et al.*: *Appl. Phys. Lett.* 97 (2007) 162909, *Jpn. J. Appl. Phys.* 47 (2008) 7623. 5) Y. Kitanaka *et al.*: *Jpn. J. Appl. Phys.* 49 (2010) 09MC06, *Ferroelectrics* 414 (2011) 24.

E-P09-M

Excess potassium and microstructure control for producting dence $KNbO_3$ ceramics

S. Sato*, Y. Hiruma, H. Nagata and T. Takenaka
Faculty of Science and Technology, Tokyo University of Science, 2641 Yamazaki, Noda, Chiba 278-8510, Japan
E-mail: nagata@takenaka.ee.noda.tus.ac.jp

Potassium Niobate, $KNbO_3$[KN], ceramics attracted considerable attentions as a candidate material for lead-free piezoelectric applications. This is because single-crystal KN has a large piezoelectricity and a hig Curie point[1]. However, because of the poor sinterability of $KNbO_3$ ceramics by conventional firing in air, the are few reports on the electrical properties of KN ceramics. Recently, we have successfully fabricated dence K ceramics derived from $KHCO_3$ as a starting material. Then, it is found that dense KN ceramics with hig resistivity were prepared in the K excess compositions rather than the stoichiometric composition. In this stud we tried to understand a mechanism of the densitication for K excess KN ceramics from a viewpoint microstructure control.

$K_{(1+x)}NbO_3$(KN-x, x=0, 0.07, 0.15) ceramics were prepared by a conventional ceramic fabrication process usi $KHCO_3$ as starting materials. Microstructures of prepared samples were observed by SEM. The samples $2\times2\times5$ mm^3 for piezoelectric measurements were poled in a silicone oil bath. Piezoelectric properties of KN were measured by a resonance-antiresonance method using an HP 4294A impedance analyzer.Figure 1 sho the fractured surfaces of sintered KN ceramics, for KN-0 and KN-0.07. The grain sizes of KN-0 are larger th those of KN-0.07 ceramics. Also, each grain of KN-0 ceramics has facet structure. Therefore, there are a lot of pores between the grains with facet structure. On the other hand, KN-0.07 ceramics shows homogeneous microstructure. For the result, considerably effect of excess K is related to the grain growth. Additionally, we found that the difference of grain growth is originally come from the grain growth during the calcination.

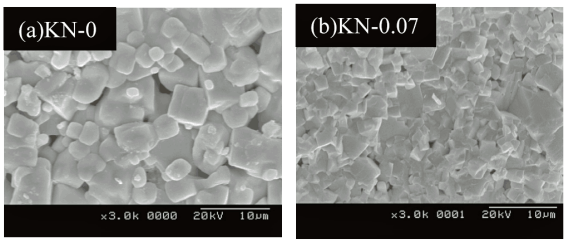

Fig. 1. Fractured surfaces of sintered KN ceramics (a) KN-0 and (b) KN–0.07

1) S. Wada et. al: *Jpn. J. Appl. Phys.*, **40** (2001) 5690.

Session F

F-09-D

Selective modification of porous nano-carbon network/Alumina (NCN/Al_2O_3) composite by ultrafine Pt nanoparticles

Chunxi Hai, Takashi Shirai and Masayoshi Fuji *

Ceramics Research Laboratory, Nagoya Institute of Technology, 3-101-1, Hommachi, Tajimi, Gifu, Japan

*fuji@nitech.ac.jp

Binary porous composite nano-carbon networks/Alumina (NCN/Al_2O_3) was modified with uniformly dispersed Pt nanoparticles employing microwave irradiation method. NCN/Al_2O_3 was fabricated by the combination of gel-casting and high temperature reductive sintering (HTRS) in Ar. By HTRS, well-gelled polymer paths in green body were converted to nano-carbon networks (NCN). Crystal structure of NCN in binary composite was confirmed to be graphitic as confirmed by Raman spectroscopy (Fig.1).

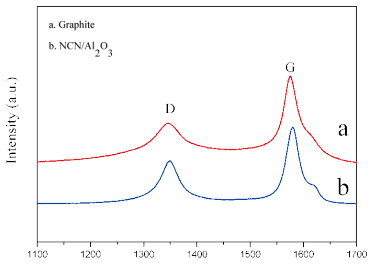

Fig.1. Raman spectroscopy of (a) Graphite and (b) NCN/Al_2O_3

Considering the unique structure of NCN/Al_2O_3 and the merits of microwave-assisted heating method, uniformly dispersed Pt nanoparticles were selectively deposited onto the surface of matrix. Two kinds of methods have been developed for selective deposition, namely conventional reductive reaction (CRR) and microwave-assisted reductive reaction (MRR). Comparing with CRR, ultrafine Pt particles via MRR deposition is attributed to polarization of NCN with graphitic structure resulting heat. The heat was attributed to dielectric loss of substrates.

F-P04-B

Functional Accumulation of Colloidal Particle and Chemical Modified Graphene

H. Endo[*1,2], K. Kono[1], F. Kono[1], T. Mizuno[1] and T. Kawai[1,2]

[1] Department of Industrial Chemistry, Tokyo Univ. of Science, 1-3 Kagurazaka, Shinjuku 162-8601, JAPAN.

[2] Center for Colloid and Interface Science (CCIS), Tokyo Univ. of Science, 1-3 Kagurazaka, Shinjuku 162-8601, JAPAN.

*endo@ci.kagu.tus.ac.jp

Lithium-ion batteries have become increasingly popular over the last two decades due to demand for portable energy storage devices. Increasing the amount of electrode/electrolyte interface to enhance charge transport has the potential to improve the electrochemical properties of the lithium ion batteries. The use of hierarchical porous electrode materials offers an efficient method for increasing the interfacial area and decreasing the lithium ion diffusion distance, allowing for fast charge transport and improved power capability. Herein, we propose that fabrication of porous structure using graphene nanosheet and colloidal particle.

Graphene oxide (GO) was synthesized from graphite powder by a modified Hummers method, and then GO-NH_2 was prepared by mixing GO and ethylenediamine. Core-shell structured polystyrene (PS) / GO-NH_2 microspherical particles (PS/GO-NH_2) were synthesized by adsorbing positively charged GO-NH_3^+ on negatively charged PS surface through a electrostatic interaction. After arrangement of this hybrid particle on substrate, PS only was dissolved by chloroform, resulting formed porous grapheme structure.

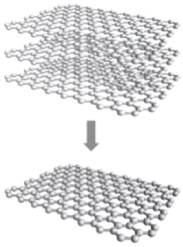

Fig. 1: Schematic illustration of graphene

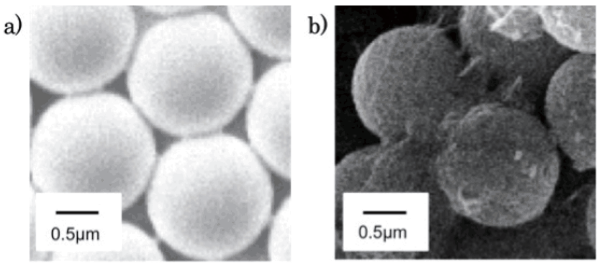

Fig. 2: SEM images of a) PS and b) PS/GO-NH_2 composite.

Session G

G-12-G

High efficient electron emission from polycrystalline diamond particles with fine facets

K. Nose* and Y. Mitsuda

Institute of Industrial Science, The University of Tokyo. nose@iis.u-tokyo.ac.jp

Much attention has been paid to high efficient electron emitters that can be applicable to cold cathodes. Second generation illuminations and electron sources for research instruments can be achieved by these electron emitters composed of commonly-available elements and materials. In this study, we have demonstrated stable electron emission at low electric fields from unique structured polycrystalline diamond particles (PDPs).

PDPs were synthesized by bias-enhanced (Vdc=-230 V) nucleation method in microwave plasma chemical vapor deposition at 6 kPa using a three-step deposition procedure [1]. PDPs were surrounded by tiny and sharp crystal apexes on their surfaces as shown in Fig. 1. Raman spectroscopy exhibited that PDPs were composed of diamond and graphitic carbon phases. Electron emission properties of PDPs/diamond cathode were measured in an ultrahigh vacuum. Electron emission was detected at extremely low-electric fields (0.8 V/μm) from PDPs with a surface of more apexes as shown in Fig. 1 (a). The emission was maintained for over 24 hours. PDPs with more simple structure (b) resulted in higher threshold electric fields. On the other hand, single crystalline diamond particles showed no emission up to 2.5 V/μm. Annealing the PDP sample in air caused no degradation of emission properties, indicating that the surface termination by oxygen scarcely affected the electric properties of the surface.

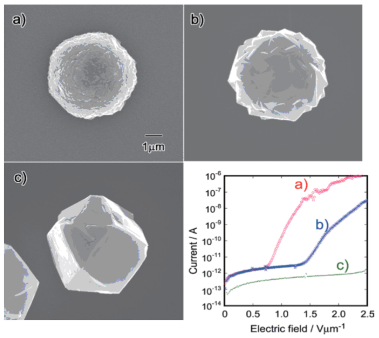

Fig. 1. Structures and electron field emission properties of (a,b) polycrystalline and (c) single crystalline diamond particles

References. [1] K. Nose et al., *Diamond and Relat. Mater.*, **20**, pp. 687-692 (2011).

Session H

H-P15-G

Ab intio local stress calculation on 4d transition metal surface

Y. Shiihara*, M. Kohyama[1], and S. Ishibashi[2]

Institute of Industrial Science, The University of Tokyo, 4-6-1 Komaba, Meguro-ku, Tokyo 153-8505, Japan, [1] Research Institute for Ubiquitous Energy Devices (UBIQEN), National Institute of Advanced Industrial Science and Technology (AIST), 1-8-31, Midorigaoka, Ikeda, Osaka 563-8577, Japan, [2] Nanosystem Research Institute (NRI) "RICS", AIST, 1-1-1 Umezono, Tsukuba, Ibaraki 305-8568, Japan, * nori@telu.iis.u-tokyo.ac.jp

Surface has a different strain or stress state from the bulk because of the lower coordination of surface atoms. On late transition metal surfaces, it has been postulated that stress or strain can be used to improve bonding properties between some adsorption atoms and the surfaces[1-2] as it happens on bimetallic surfaces with mismatch stress. To elucidate how stress is correlated with the chemisorption properties, it is important to reveal the mechanism how the intrinsic stress occurs on the transition metal surfaces.

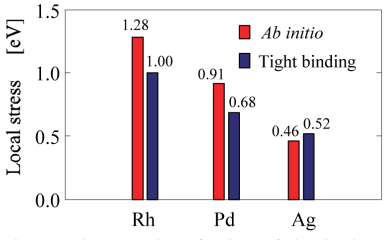

Fig. 1 Local stress on the surface layer of Rh, Pd and Ag.

In this study we investigate the *ab initio* local stress distribution[3] inside the fcc (111) surfaces of 4d transition metals, Rh, Pd, and Ag. The obtained layer-by-layer stress provides us a detailed insight into the mechanism of the stress because they can be directly compared with the physical quantities defined on each atomic layer such as partial density of states (PDOS). To compare with the *ab initio* local stress, a tight-binding stress on the basis of the second-moment theory is formulated. Figure 1 shows good agreement between the *ab initio* and tight-binding local stresses on the surface top layer, especially in Ag. This result indicates that the stress on the surface can be partially expressed using the tight-binding theory while the past theoretical studies regard only charge redistribution as the origin of the surface stress. Considering the PDOS on the surface layer, we also show the change of *d-d* bonding character can play an additional role in the origin of the stress in Rh and Pd where a certain amount of discrepancy is observed in Fig. 1.

References : 1) M. Mavrikakis, B. Hammer, and J. Nørskov, Phys. Rev. Lett. 81, 2819 (1998). 2) Y. Uesugi-Saitow and M. Yata, Phys. Rev. Lett. 88, 256104 (2002). 3) Y. Shiihara, M. Kohyama, and S. Ishibashi, Phys. Rev. B 81, 075441 (2010).

H-26-M

Phase Diagram and Band Gap of $CuInSe_2$–$CuGaSe_2$ and $CuInSe_2$–$CuAlSe_2$ Systems

Y. Soda, Y. Kumagai, F. Oba*, A. Seko, and I. Tanaka
Department of Materials Science and Engineering, Kyoto University, Sakyo, Kyoto 606-8501, oba@cms.mtl.kyoto-u.ac.jp

The pseudobinary alloys of $CuInSe_2$ (CIS) and $CuGaSe_2$ (CGS) with the chalcopyrite structure, $CuIn_{1-x}Ga_xSe_2$ (CIGS), are utilized as light absorbers in CIGS thin-film solar cells. The formation of the CIGS alloys enables us to control the band gap for increasing the cell efficiency. $CuIn_{1-x}Al_xSe_2$ (CIAS), which is an alloy of CIS and $CuAlSe_2$ (CAS), has also been studied as an alternative absorber material. A great impact of the characteristics of CIGS and CIAS on the cell efficiency has stimulated investigations of the phase-transition and phase-separation behavior and the composition dependence of the band gap, but the understanding is limited. In this study, the temperature-composition phase diagrams and band gaps of the CIS–CGS and CIS–CAS systems are determined using a combination of first-principles calculations, cluster expansion (CE), and Monte Carlo (MC) simulations.

The total energies and band gaps of 43 ordered structures in 64-atom supercells were calculated using an HSE06 hybrid functional as implemented in the VASP code. Effective cluster interactions were estimated so that they reconstruct the total energies and band gaps. Thermodynamic averages of atomic configurations and band gaps were obtained via semi-grand canonical MC simulations using 4096-atom supercells. Phase boundaries were determined from the semi-grand potentials estimated by the thermodynamic integration. The CE and MC simulations were performed using the CLUPAN code.

Figure 1(a) shows the calculated phase diagram for the CIS–CGS system. The binodal curve gives a phase-separation critical temperature of ~ 420 K. A similar phase diagram has been obtained for the CIS–CAS system. The calculated composition dependence of the band gap of CIGS at the ideal disorder state is shown in Fig. 1(b). A nearly quadratic behavior, i.e., band bowing, is recognized as often found for semiconductor alloys. For both CIGS and CIAS, the configurational contributions to the temperature dependence of band gaps, which lead to the dependence on the temperature before quench, are found to be rather small and the band gaps are generally close to those at the ideal disorder state.

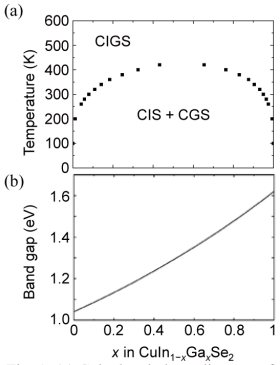

Fig. 1. (a) Calculated phase diagram of the CIS–CGS system and (b) the band gap of CIGS at the ideal disorder state.

H-17-G

Determination of Atomic Configurations and Lithium-Ion Conduction Mechanisms in LISICON-based Solid Electrolytes by First-Principles Calculations

K. Fujimura[1,2)*], A. Kuwabara[1)], H. Moriwake[1)], K. Nobuhara[3)], Y. Koyama[4)] and I. Tanaka[2,1)]
[1)] Nanostructures Research Laboratory, Japan Fine Ceramics Center, Atsuta-ku, Nagoya 456-8587, Japan, [2)] Department of Materials Science and Engineering, Kyoto University, Sakyo-ku, Kyoto 606-8501, Japan, [3)] Higashifuji Technical Center, Toyota Motor Corporation, Susono, Shizuoka 410-1193, Japan, [4)] Office of Society-Academia Collaboration for Innovation, Kyoto University, Sakyo-ku, Kyoto 606-8501, Japan.
*k_fujimura@jfcc.or.jp

Toward the development of next-generation all solid rechargeable batteries, it is essential to further improve ionic conductivity of solid electrolytes. The name LISICON, which stands for Lithium Super Ionic Conductor, is a member of the solid solution, $Li_{2+2x}Zn_{1-x}GeO_4$ ($0 \le x \le 1$). LISICON is a classical Li^+ ion conductor, however theoretical investigation has not been done enough yet. There are the β-form, the γ-form and the Li_4SiO_4-form as crystalline polymorph according to temperature and stoichiometry. In this work, we employ the first-principles method to predict accurately relationship between energy surface and various atomic configurations and to elucidate Li^+ ion conduction mechanism.

The calculations were performed using the projector augmented wave (PAW) method with generalized gradient approximation as implemented in the VASP code. Figure 1 shows total energies which were calculated systematically for 1748 atomic configurations in Li_4GeO_4 (x=1). The most stable configuration could reproduce the structure of Li_4GeO_4 reported experimentally. Moreover, activation energy for Li^+ ion conducting was evaluated by nudged elastic band (NEB) method. We found that an interstitialcy mechanism, involving cooperative motions of an excess Li^+ ion at octahedral site and a neighboring Li^+ ion at tetrahedral site, decreases energy barrier drastically.

This work was supported by Li-EAD project of New Energy and Industrial Technology Development Organization (NEDO), Japan.

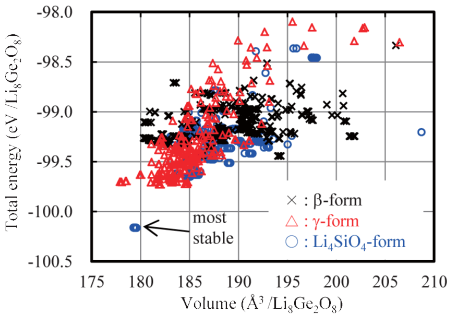

Figure 1. The relationship between volume and energy of atomic configurations in Li_4GeO_4.

References : 1) H. Y-P. Hong, *Mat. Res. Bull.* **13**, 117 (1978).
2) P. G. Bruce and A. R. West, *Mat. Res. Bull.* **15**, 379 (1980).
3) H. Völlenkle and A. Wittmann, Naturwissensch. 54, 441(1967).

H-P23-D

X-ray absorption near-edge structure analysis of $Pr_{1-x}A_xCoO_{3-\delta}$ (A = Ca and Sr) with the aid of the first-principles calculations

T. Yoshioka* and T. Yamamoto
Faculty of Science and Engineering, Waseda University, 3-4-1 Shinjuku-ku, Tokyo 169-8555, Japan
*t-yoshioka@ruri.waseda.jp

Rare-earth cobaltate doped with alkaline-earth ions, $R_{1-x}A_xCoO_{3-\delta}$ (R = rare-earth, A = alkaline-earth), have been extensively studied, because they have unique electronic and magnetic properties such as colossal magnetoresistance and metal-insulator transition[1-3]. In order to understand such properties, it is essential to know the charge state in these materials. When the alkaline-earth ions are substituted at rare-earth site in $RCoO_3$, one or both of the followings should occur to keep the system electrically neutral, i) Co and/or Pr ions controls charge balance of the system, i.e., $Co^{3+} \rightarrow Co^{4+}$ or $Pr^{3+} \rightarrow Pr^{4+}$, ii) oxygen vacancy is created. However, these mechanisms of charge compensation have not yet been thoroughly investigated for these materials.

In the present study, the electronic structure analysis of Pr ions and Co ions in $Pr_{1-x}A_xCoO_{3-\delta}$ (A = Ca, Sr) are systematically carried out here by the X-ray absorption near-edge structure (XANES) measurements. Pr-L_3 XANES spectra of $Pr_{1-x}A_xCoO_{3-\delta}$ are almost identical, and the results indicate that Pr is trivalent. And observed Co-L_3 XANES spectra of $Pr_{1-x}Ca_xCoO_{3-\delta}$ are shown in Fig. 1, which were deconvoluted into three peaks using Gaussian function. The fine structure of Co-L_3 XANES spectra of $Pr_{1-x}Ca_xCoO_{3-\delta}$ continuously changes depending upon the concentration of doped Ca^{2+} ions, i.e., relative intensity of peak A to B increases and relative intensity of peak C to B decreases as increment of doped Ca^{2+} ions concentration. These results indicate that distribution of Co-3d band in $Pr_{1-x}Ca_xCoO_{3-\delta}$ changes depending upon the concentration of doped Ca^{2+} ions. The first-principles calculations were also carried out to explain these XANES results.

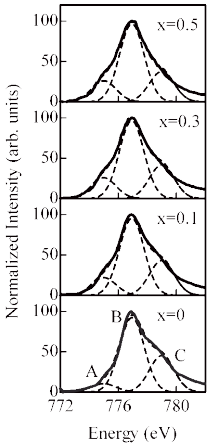

Fig. 1 Co-L_3 XANES spectra of $Pr_{1-x}Ca_xCoO_{3-\delta}$.

References: 1) S. Tsubouchi et al., Phys. Rev. B **69**, 144406 (2004). 2) H. Masuda et al., J. Phys. Soc. Jpn. **72**, 873 (2003). 3) V. Golovanov and L. Mihaly, Phys. Rev. B **53**, 8207 (1996).

H-06-G

Molecular Dynamics Simulation of Nanoindentation Using EAM Potential for Fe with Pseudo-Hydrogen Effects

R. Matsumoto[1)*], S. Seki[2)], S. Taketomi[3)] and N. Miyazaki[1)]
[1)]Department of Mechanical Engineering and Science, Graduate School of Engineering, Kyoto University, Yoshida-Honmachi, Sakyo-ku, 606-8501, Kyoto, Japan, [2)]Graduate Student, Department of Mechanical Engineering and Science, Graduate School of Engineering, Kyoto University, [3)]Department of Mechanical Engineering, Graduate School of Science and Engineering, Saga University, 1 Honjo-machi, Saga-city, 840-8502, Saga, Japan, *matsumoto@solid.me.kyoto-u.ac.jp

A lot of studies have reported that solute hydrogen atoms and lattice defects have strong interactions, and that hydrogen atoms significantly change the stability and/or mobility of lattice defects. Although molecular dynamics (MD) simulations can treat complicated interactions of various lattice defects, the time scale is insufficient to treat hydrogen diffusion so as to influence the lattice-defect generation and cooperative motion of hydrogen atoms and lattice defects. Here we use an embedded atom method (EAM) potential for Fe with pseudo-hydrogen effects on lattice-defect energies[1)] and performed MD simulations of nanoindentation.

The deformation behaviors during nanoindentation are shown in Fig. 1. Here, only non-bcc structures are shown, and they are colored using Adaptive template analysis: ATA[2)]; red is surfaces, blue is stacking faults and green is vacancy. The pure-Fe case was calculated using EAM potential developed by Mendelev et al.[3)]. Our MD results showed that hydrogen induces earlier dislocation burst, and enhances generation of many vacancies all over the simulation model.

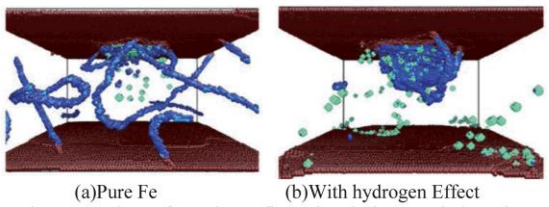

(a)Pure Fe (b)With hydrogen Effect

Fig.1. Snapshots of atomic configuration during nanoindentation (displacement = 2.28 nm)

References:1) S. Seki et al., Journal of the Society of Materials Science, Japan, (2011) (In printing). 2) F. A. Sapozhnikov et al., Russian Journal of Physical Chemistry B, 2, 238-45 (2008). 3) M. I. Mendelev et al., Philosophical Magazine, 83, 3977-94 (2003).

Session I

I-20-M

Conformation and Intermolecular Interaction of Cycloamylose Tris(phenylcarbamate) in Good and Theta Solvents

N. Asano, K. Terao*, S. Kitamura[1)] and T. Sato
Department of Macromolecular Science, Osaka University, 1-1 Machikaneyama-cho, Toyonaka, Osaka 560-0043, Japan, [1)]Graduate School of Life and Environmental Sciences, Osaka Prefecture University, 1-1 Gakuen-cho, Nakaku, Sakai, Osaka 599-8531, Japan, *kterao@chem.sci.osaka-u.ac.jp

We synthesized a rigid cyclic polymer, that is, cycloamylose tris(phenylcarbamate)(cATPC, Fig. 1), from rather flexible cycloamylose. Light and synchrotron-radiation small-angle X-ray scattering measurements were made on five cATPC samples in two good solvents (1,4-dioxane and 2 ethoxyethanol) and three theta solvents [4-methyl-2-pentanone (MIBK), ethyl acetate (EA), and methyl acetate] to determine the conformation in solution as well as the second virial coefficient A_2. We found that cATPC behaves as a rigid cyclic chain in all the five solvents but the local conformation in MIBK is appreciably different from that for linear ATPC. A further interesting finding is that A_2 for cATPC in MIBK at the theta temperature is negative whereas that in EA is positive, the latter A_2 value which should be due to the topological interaction. This anomalous behavior of A_2 in MIBK is possibly because of the difference in the local conformation between cATPC and linear ATPC in MIBK.

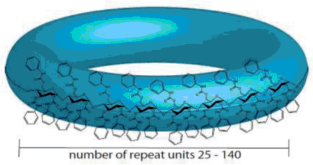

Fig. 1. Chemical structure of cycloamylose tris(phenylcarbamate).

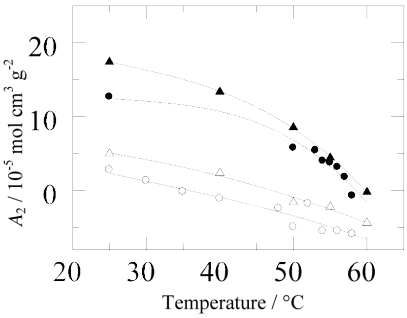

Fig. 2. Temperature dependence of A_2 for amylose tris(phenylcarbamate) (filled circles and filled triangles) and cycloamylose tris(phenylcarbamate) (unfilled circles and unfilled triangles) in MIBK.

I-08-M

Dielectric Measurements on Human Skin of Various Body Parts by Time Domain Reflectometry Using Open-End Probes with Different Diameters

H. Kamata*, C.Yamamoto, R. Kita, N. Shinyashiki, S. Yagihara
Graduate School of Science, Tokai University, Hiratsuka, Kanagawa 259-1292, *0bsnm003@mail.tokai-u.jp

Human skin consists of three layers of the epidermis, dermis, and subcutaneous tissues from the body surface. Skin protects human body from exogenous stimuli and keeps the body at just right temperature. In order to evaluate the human skin in vivo, non-invasive measurements are very important. Time Domain Reflectometry (TDR) is an effective tool to evaluate water contents and the dynamical behaviors of water included in the human skin. We performed dielectric measurements for human skin of various parts of a body in a frequency range from 100MHz to 20GHz by TDR using open-end coaxial probes with five different diameters. A relaxation process due to reorientation of free water molecules was observed in GHz frequency range. Figure.1 shows a relationship of the relaxation strength thus obtained and the thickness of the epidermis reported in literatures for different probes with outer diameter 0.86, 1.2, 2.2, 3.6, and 6.3mm. Larger values of the relaxation strength were obtained for thinner epidermis and also for probes with larger diameters. It is well known that the water content in epidermis was less than that in dermis. Therefore the larger penetration depth of the electric field with larger-diameter electrodes increases information of the dermis. The single logarithmic plot of figure 1 was prepared for an assumption of a single decay function of the relaxation strength against d values. Straight lines tentatively drawn for respective electrodes indicate adequacy of the assumption. Here values of the relaxation strength at zero thickness of skin were about 50 for larger electrodes because of corresponding water content of 70%. TDR measurement is an effective technique to evaluate skin condition.

References: 1) M. Hashimoto, T. Goto, N. Shinyashiki, S. Yagihara, The Tokai journal of sports medical science 19, 53-62, 2007

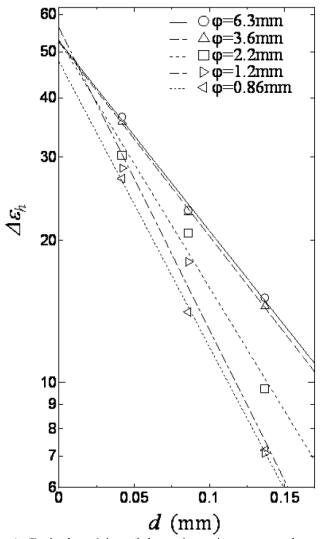

Fig. 1. Relationship of the relaxation strength and the thickness of the epidermis with the probe outer diameter 0.86, 1.2, 2.2, 3.6, and 6.3mm

I-P13-M

Lyotropic Liquid Crystallinity of Amylose Alkylcarbamates in Various Solvents

K. Oyamada, K. Terao*, S. Kitamura[1)] and T. Sato

Department of Macromolecular Science, Osaka University, 1-1 Machikaneyama-cho, Toyonaka, Osaka 560-0043, Japan, [1)] Graduate School of Life and Environmental Sciences, Osaka Prefecture University, 1-1 Gakuen-cho, Nakaku, Sakai, Osaka 599-8531, Japan, *kterao@chem.sci.osaka-u.ac.jp

Rigid polymers may form lyotropic liquid crystal in concentrated solutions. Amylose alkylcarbamates have very high stiffness in tetrahydrofuran (THF), ethyl lactate (EL) and 2-buthanol. However, no liquid crystal phase has been reported for these polymer systems so far. Recently, we found liquid crystal phases in amylose alkylcarbamates solutions. Phase separation experiment and polarizing microscope observation as well as X-ray diffraction and circular dichroism measurements were made on concentrated THF and ethyl lactate solutions of amylose alkylcarbamates to determine the phase diagram and the structure of each phase. X-ray diffraction was also measured on the liquid crystal phase of the 2-buthanol solution. We found that THF solution forms transparent left-handed cholesteric phases, of which phase diagrams were well explained by the current theory. On the other hand, EL and 2-buthanol solutions were opaque and showed X-ray diffraction peaks which correspond to the length of a single extended ATBC chain, indicating the formation of a smectic phase. Additional sharp peaks at wider angles were also found. The diffraction data for samples oriented by magnetic field indicates that the peaks correspond to the inter-chain distance between ATBC molecules in the smectic phase.

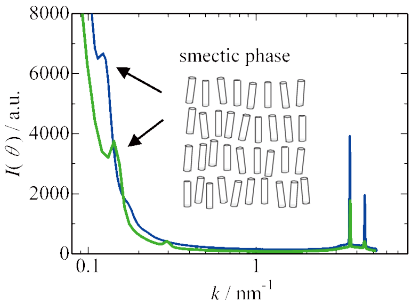

Fig. 1. X-ray diffraction profiles for an ATBC sample ($M_w = 1.33\times10^5$) in *L*-EL and another ATBC sample ($M_w = 6.03\times10^4$) in *D*-EL.

Session J

J-P01-M

Rotary phase of surface wave on gelatin gel

T. Yamomoto, Y. Yoshitake

Tokyo Denki University, Hatoyama, Hiki-gun, Saitama, 350-0394 Japan

10rmr11@ms.dendai.ac.jp

Since gels consist of two components of network and solvent, their properties are different from those of liquids and simple solids. This leads to the question as to what type of surface wave propagates on gel. The surface wave propagations are generally subject to elasticity and surface tension: The former governs the behavior in the long-wavelength range or high elasticity where the gel surface waves behave as Rayleigh waves, while the latter plays a major role in the region of short wavelength or low elasticity and Capillary waves run. In the intermediate region, gel is involved in a complex phenomenon that is troublesome from a viewpoint of measurement.

The purpose of this study is to clarify dispersion relations on gels from the viewpoint of rotary motion. Capillary waves on pure liquid surface rotate the surface elements in clockwise direction, on the contrary, Rayleigh waves on solid make anti-clockwise motion when the waves propagate to the right direction. We developed the high-speed observation system which enabled us to observe surface waves propagating on gel. As a result, we observed the gel surface waves behave liquid-like motion at low concentration (capillary wave region), and solid-like motion at high concentration (Rayleigh wave region).

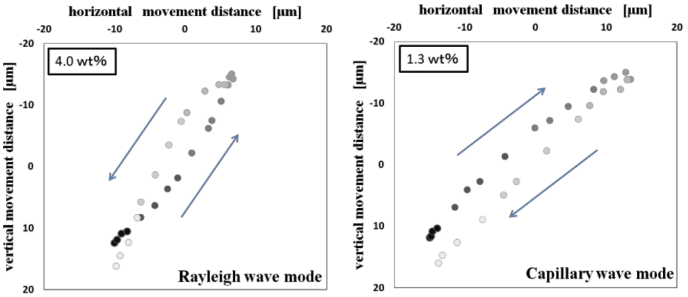

Fig. 1. Particle motion on gel surface waves. Gel surface waves turn clock wise circular at t low concentration 1.3wt%(right), anticlockwise circular at high concentration 4.0w%(left).

Session K

K-32-G

Tricolored Mechanochromic Luminescent Liquid Crystal Having a Single Luminophore

Y. Sagara and T. Kato*
Department of Chemistry and Biotechnology, School of Engineering, The University of Tokyo
Hongo, Bunkyo-ku, Tokyo 113-8656, Japan
*e-mail: kato@chiral.t.u-tokyo.ac.jp

Photoluminescent properties of molecular materials depend on the molecular assembled structures. The switching of molecular assembled structures is one of the most fascinating approaches to develop stimuli-responsive luminescent materials.[1–5] To date, various types of mechanochromic luminescent materials have been reported. We also have prepared some liquid-crystalline mechanochromic luminescent materials.[1,3–5]

In this study, we have prepared a new type of stimuli-responsive luminescent liquid crystals exhibiting three bright luminescent colors that are switched between each other by mechanical and thermal stimuli. The liquid crystal is composed of equimolar amounts of a dumbbell-shaped compound and a dendritic compound. The dumbbell-shaped compound has two dendritic groups attached to the 9,10-bis(phenylethynyl)anthracene moiety through amide groups. The mixture forms a micellar cubic phase from room temperature to 146 °C on heating. Under UV irradiation (365 nm), reddish-orange photoluminescence is observed for the micellar cubic phase. Mechanical shearing to the mixture in the cubic phase at 90 °C triggers change in luminescent color from reddish-orange to green. The mechanochromic luminescent behavior is accompanied by a shear-induced phase transition from the micellar cubic phase to the columnar phase. We have also found that the mixture exhibits the other change in luminescent color. When the mixtures in the micellar cubic or columnar phases are mechanically sheared at room temperature, the mixtures show an unidentified mesomorphic phase exhibiting yellow emission. Following proper procedures, the tri-colored luminescent pattern has been obtained at room temperature.

References: 1) Y. Sagara and T. Kato, *Nature Chem.* **2009**, *1*, 605. 2) Y. Sagara, T. Mutai, I. Yoshikawa and K. Araki, *J. Am. Chem. Soc.* **2007**, *129*, 1520. 3) Y. Sagara and T. Kato, *Angew. Chem. Int. Ed.* **2008**, *47*, 517. 4) Y. Sagara, S. Yamane, T. Mutai, K. Araki and T. Kato, *Adv. Funct. Mater.* **2009**, *19*, 1869. 5) Y. Sagara and T. Kato, *Supramol. Chem.* **2011**, *23*, 310. 6) Y. Sagara and T. Kato, *Angew. Chem. Int. Ed.* **2011**, *50*, 9128.

Acknowledgment: This work was supported by Grant-in-Aid for Scientific Research (No. 22107003) on the Innovative Areas: "Fusion Materials" (Area no. 2206) from MEXT.

K-P10-M

Realization of Biaxial Nematic and Smectic A Phases by Using Rodlike Molecules

K. Kishikawa[1)], T. Inoue*, M. Takahashi and S. Kohmoto
Department of Applied Chemistry and Biotechnology, Graduate school of Engineering, Chiba University, 1-33 Yayoi-cho, Inage-ku, Chiba 263-8522,Japan,[1)] *inouetakahiro1227@graduate.chiba-u.jp

In order to realize biaxial mesophases, we synthesized novel straight rod-like molecules (Figure 1). The compounds exhibited nematic and smecticA liquid crystal phases. We investigated their liquid crystal behaviors and superstructures by polarized optical microscopy (POM), differential scanning calorimetry (DSC), and one- and two-dimentional X-ray diffraction (XRD). Some compounds in the nematic phases showed schlieren textures with all 2-brushes in the POM under a magnetic field. Further, the XRDs of some compounds in the nematic phases showed periodicies in the direction of the moleculear long axis (Figure 2). It was strongly suggested that the molecules had a biaxially ordered superstructure in the mesophases by using strong face-to-face perfluoroarene-arene interaction. Some compounds indicated ferroelectric switching behaviors (Figure 3).

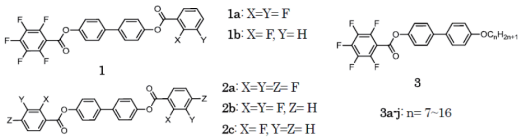

Figure 1. Molecular structures of **1**,**2** and **3**

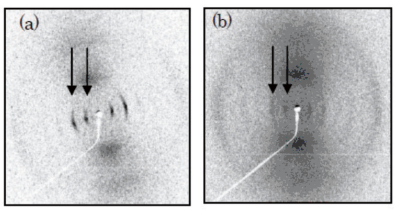

Figure 2. 2D-XRD profiles of **2a** at (a) 210°C (SmA phase) and (b) 250°C (Nematic phase).

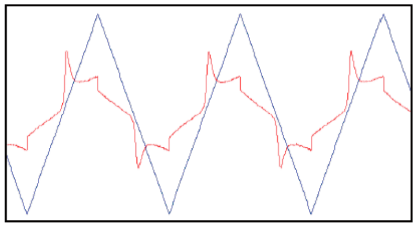

Figure 3. Ferroelectric switching behavior of **2a** (220°C, 20Hz, 150Vpp, cell gap: 5μm, area size: 1 cm×1 cm).

K-P14-M

Photorealignment behavior of micro-phase separation structure in a liquid crystalline azobenzene block copolymer thin film

Masami SANO[1)], Shusaku NAGANO[1),2)], Yuya SHINOHARA[3)], Yoshiyuki AMEMIYA[3)], and Takahiro SEKI[1)*]
[1)]Graduate School of Engineering, Nagoya University, Furo-cho, Chikusa-ku, Nagoya, 464-8603, Japan, [2)]JST-PRESTO, Department of Research Promotion, Research Division, Sanbancho Building 5F, 3-5, Sanbancho, Chiyodaku, Tokyo,102-0075
[3)]Graduate School of Frontier Sciences, University of Tokyo, 5-1-5 Kashiwanoha, Kashiwa-shi, Chiba-ken, 277-8561, Japan,
*tseki@apchem. nagoya-u. ac. jp

Recently, we have reported successful 3D photoalignment of polystyrene cylinder of micro-phase separation (MPS) structure in a photoresponsive liquid crystalline (LC) block copolymer containing poly(azobenzene methacrylate) (P5Az10MA) as the matrix by utilizing angular selective photoorientation of azobenzene chromophore with combination of thermal treatment [1]. In this paper, we proposed new MPS structure photoalignment systems without temperature control using P5Az10MA block copolymers connected to poly(butyl methacrylate) (Figure 1). The thin films were irradiated with linearly polarized light (LPL) in the liquid crystal phase at an elevated constant temperature. The resulting film exhibited the in-plane anisotropy in smectic phase and the MPS structure aligned perpendicular to the polarization plane of LPL. Moreover, we evaluated the domain structure and orientations of LC phase and microphase separation structure at the transient stage in the photoalignment process by the polarized UV-vis absorption spectroscopy, and grazing angle incidence X-ray scattering measurements.

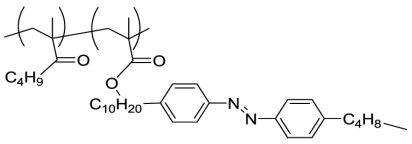

Figure 1 Chemical structure of PBMA-b-P5Az10MAs.

[1] Y. Morikawa, T. Kondo, S. Nagano, T. Seki, *Chem. Mater.* **2007** *19*, 1540.

.

K-15-G

Hybrid Structures Prepared by Electroless Plating of Self-Organized Honeycomb-Patterned Porous Films

D. Ishii[*1),2)], H. Yabu[2),3)], M. Shimomura[1),2),3)]
[1)] WPI-AIMR, Tohoku University, 2-1-1, Katahira, Aoba-ku, Sendai 980-8577 Japan, [2)] CRESR-JST, 4-1-8 Hon-cho, Kawaguchi 332-0012, Japan, [3)] IMRAM, Tohoku University, 2-1-1, Katahira, Aoba-ku, Sendai 980-8577 Japan,
[*]dishii@tagen.tohoku.ac.jp

Several types of metal–polymer hybrid structures were prepared by electroless plating of self-organized honeycomb-patterned porous films[1)]. The polystyrene honeycomb film was fabricated by a template method of hexagonally ordered condensed water droplets, and composed of a micrometric porous array and nanometric pillar structures that hold top and bottom porous layers together. Chemical adhesion of palladium catalysts for nickel electroless plating was controlled by difference of wettability of the honeycomb structures. After electroless plating and peeling off the top layer of the honeycomb film, various kinds of the metal–polymer hybrid films such as metal-coated honeycomb-patterned polymer films, metal-coated pillar-structured polymer films, ring-like-structured metal in the honeycomb-patterned polymer film, ball-like-structured metal array in the honeycomb-patterned polymer film, and dome-like-structured metal in the pillar-structured polymer film were obtained.

We will demonstrate that microdroplet handlings, such as transfer between superhydrophobic surfaces, separation by small electric energies and so on, achieved by using the hybrid structures possessing characteristic wettabilities. The microdroplet handling is important for further understanding of superhydrophobic surfaces and application in microfluidic devices.

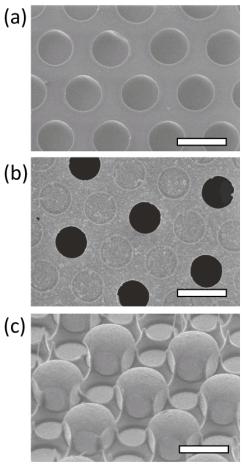

Fig. 1. SEM image of self-organized honeycomb-patterned porous films (a), metal-polymer hybrid structures before (b) and after (c) peeling .

References: 1) H. Yabu, M. Takebayashi, M. Tanaka, M. Shimomura, *Langmuir*, 21, 3235–3237 (2005).

Session L

L-09-M

Molecular Arrangement of Organo-modified Aluminosilicate in Langmuir-Blodgett Films and Mixed Monolayer Behavior with Biodegradable Polymers.

Jun-ichi Kusaka[1),2)], Shuntaro Arai[3)], Munehiro Kubota[4)], Kei-ichi Kurosaka[4)], and Atsuhiro Fujimori[2),*]

[1)]Graduate School of Science and Engineering, Yamagata University., Jonan 4-3-16, Yonezawa, Yamagata, 992-8510, Japan, [2)]Graduate School of Science and Engineering and [3)]Department of Functional Materials Science, Faculty of Engineering, Saitama University, Shimo-okubo 255, Sakura-ku, Saitama, 338-8570, Japan, [4)]Kunimine Industries Co., Ltd, Iwaki, Fukushima, 972-8312, Japan. *fujimori@fms.saitama-u.ac.jp

We investigated molecular arrangement of organo-modified montmorillonite with high surface coverage in Langmuir-Blodgett films (LB) by out-of plane and in-plane X-ray diffraction (XRD) mesurements. In addition, surface morphology of mixed monolayer for the organo-modified montmorillonite and several biodegradable polymers (ex. poly(L-lactide), *abbrev.* PLLA) was also observed by atomice force microscopy (AFM). From the results of in-plane XRD of multilayers of organo-modified montmorillonite formed by LB method, it is found that two-dimensional lattice of hydrocarbons on the montmorillonite surface is formed. These hydrocarbons of organo-modified reagent packed hexagonally (Fig. 1). From these experimental findings, it is concluded that the LB technique enables formation of densely packed organo-modified alminosilicate monolayer at the water surface. Further, in the case of mixed monolayer system of organo-modified clay with high surface coverage and biodegradable polymers, apparently miscible surface was observed by AFM at mesoscopic scales whereas formation of obvious phase separated structure of that with low surface coverage (Fig. 2).

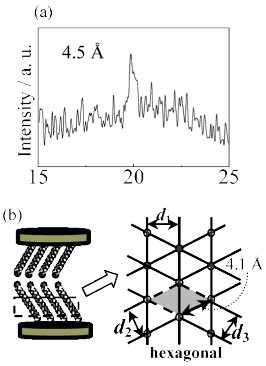

Figure 1 (a)In-plane XRD profile of LB film for organo-modified montmorillonite with high surface coverage. (b) Schematic illustration of two-dimensional lattice of hydrocarbon units

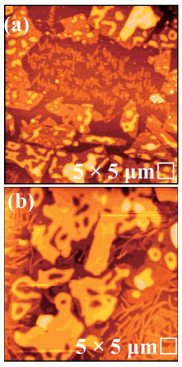

Figure 2 AFM images of mixed monolayer for PLLA and organo-modified Montmorillonite with (a)low and (b) high surface coverage.

Reference: Fujimori, A.; Kusaka, J.; Nomura, R., *Polym. Eng. Sci.*, **2011**, *51*, 1099.

L-20-M

Fabrication and characterization of non-labeled IgA immunoseonsor

R. Ohno[1)], H. Ohnuki*[1)], H. Wang[1)], T. Yokoyama[1)], D. Tsuya[2)], M. Izumi[1)]

[1)]Tokyo Univ. of Marine Sci. and Tech., 2-1-6 Etchujima Koto-ku, Tokyo 135-8533, Japan, [2)]National Institute for Materials Sciense, 1-2-1 Sengen, Tsukuba, Ibaraki 305-0047, Japan,

*ohnuki@kaiyodai.ac.jp

In recent years, great progress in thin film production technologies such as vacuum deposition, ion plating, sputtering, chemical vapor deposition, or pulse laser deposition has opened new opportunities for assembling electrochemical immunosensors. Interdigitated microelectrode (IDE) having a series of parallel micro-band electrodes with micro-bands connected together, offer advantages such as rapid reaction, high sensitivity, large electrode aspect ratio and great signal-to-noise ratio.

We succeeded in fabrication of non-labeled immuno globulin A (IgA) immunosensor by using IDE. In the fabrication of the sensor, anti-body of IgA (Anti-IgA) was bonded to the 3-mercaptopropionic acid (MPA) that was immobilized by self-assembled-monolayer (SAM) technique on the Au electrodes through the covalent combination of amino groups in Anti-IgA and carboxyl on the MPAs.

After residual unreacted active sites were blocked by bovine serum albumin (BSA), the IgA immunosensor was fabricated.

Measurement was performed by the electrochemical impedance spectroscopy (EIS) method. EIS is a powerful method for electrochemical sensing of biological binding event such as antigen-antibody reaction at surfaces. By measuring the frequency dependence of electrical impedance, EIS provides information that can be used to separate the response of complicated inter-faces. The nyquist plots of impedance spectra are shown in Fig. 1. The diameter of the nyquist increasing with the addition of IgA and the reaction was saturated on the order of 100 ng/ml. The measurable concentration range of the sensor was found to be between 0.1 ng/ml to 100 ng/ml.

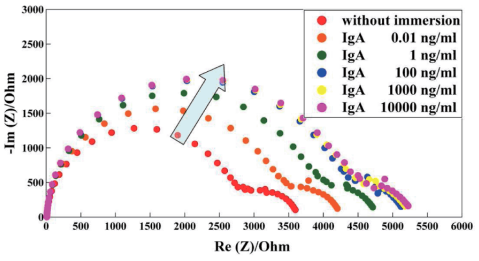

Fig. 1 Nyquist plots of the sample immersed in different IgA concentrations.

L-16-M

Fabrication of Solution-Processable Organic Material Films on Wettability-Patterned Surfaces Using O/W Emulsion

Y. AKIYOSHI*, S. WATANABE, M. MATSUMOTO
Dept. Mater. Sci. Technol., Tokyo Univ. Science. Yamazaki 2641, Noda 278-8510, Japan
*akiyoshi_8@matsulab.net

Wettability-patterned surfaces allow us to fabricate patterned solution-processable organic material films with low cost, using the adsorption of molecules from the solutions. However, conventional methods such as spin-coating have intrinsic problems of excessive consumption of the solutions for the fabrication of the films. In this study, we discuss a new technique to form functional organic films on wettability-patterned surfaces using oil/water emulsion.

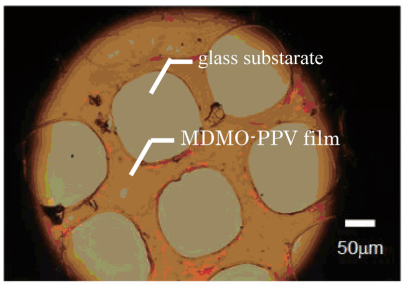

Figure 1. Optical microscope image of an MDMO-PPV film on the wettability-patterned surface.

Self-assembled monolayers (SAMs) of hexamethyldisilazane (HMDS) were formed by immersing glass substrates in HMDS. Wettability-patterns were formed on the glass substrates by the exposure to a UV/ozone atmosphere through a shadow mask to remove the SAMs of HMDS. The emulsion was prepared by adding toluene solution of poly[2-methoxy-5-(3',7'-dimethyloctyloxy)-1,4-phenylenevinylene] (MDMO-PPV) to water, followed by ultrasonication. The wettability-patterned substrates were immersed in the emulsion to form MDMO-PPV films on the SAM of HMDS.

As shown in Figure 1, the MDMO-PPV film is selectively formed on the SAM of HMDS constituting the hydrophobic part of the surface. The thickness of the MDMO-PPV film was estimated to be about 136 nm using laser microscopy. These results demonstrate the formation of organic functional material films on wettability-patterned surfaces using oil/water emulsion. In the presentation, we will also discuss the patterning of water-soluble organic materials using emulsion.

Session M

M-P27-M

Enhanced Photocatalytic Activity of $(AgIn)_xZn_{2(1-x)}S_2$ Nanoparticles Immobilized on SiO_2-Coated Au Particles

T. Takahashi[1)], K. Okazaki[1)], A. Kudo[2)], S. Kuwabata[3)], and T. Torimoto[1)*]
[1)] Graduate School of Engineering, Nagoya University, Chikusa-ku, Nagoya 464-8603, Japan. [2)] Tokyo University of Sience, 1-3 Kagurazaka, Shinjuku-ku, Tokyo 162-8601, Japan. [3)] Graduate School of Engineering, Osaka University, Suita, Osaka 565-0871, Japan. *torimoto@apchem.nagoya-u.ac.jp

Metal particles of Au or Ag exhibit the localized surface plasmon resonance (LSPR) peaks that produce an intense electric field around the particles. It has been reported in our previous paper[1)] that the photocatalytic activity of CdS nanoparticles was enhanced by the immobilization on Au core/SiO_2 shell (Au/SiO_2) particles due to the LSPR-induced electric fields around Au particles. In this study, we investigated the photocatalytic activity for H_2 evolution of $(AgIn)_xZn_{2(1-x)}S_2$ solid solution nanoparticles and their enhancement in the combination with Au/SiO_2 particles.

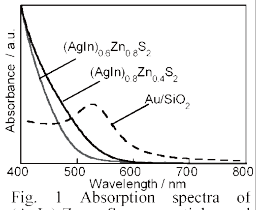

Fig. 1 Absorption spectra of $(AgIn)_xZn_{2(1-x)}S_2$ nanoparticles and Au/SiO_2 particle.

$(AgIn)_xZn_{2(1-x)}S_2$ nanoparticles were synthesized by thermal decomposition of precursor in oleylamine,[2)] followed by modified with mercaptopropyltrimethoxysilane (MPTS). By hydrolysis of this MPTS, $(AgIn)_xZn_{2(1-x)}S_2$ nanoparticles were deposited on Au/SiO_2 core-shell particles. Figure.1 shows the absorption spectra of $(AgIn)_xZn_{2(1-x)}S_2$ nanoparticles prepared with x=0.6 and 0.8 and Au/SiO_2 particles used. Photocatalytic activity for H_2 evolution was investigated by irradiating the photocatalysts suspended in a 2-propanol-water mixed solution.

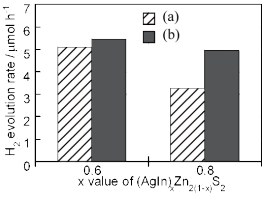

Fig. 2 Photocatalytic H_2 evolution rate. (a) $(AgIn)_xZn_{2(1-x)}S_2$ nanoparticles (b) $(AgIn)_xZn_{2(1-x)}S_2$-loaded on Au/SiO_2 nanocomposites.

TEM measurement revealed that $(AgIn)_xZn_{2(1-x)}S_2$ nanoparticles (Size: 4 nm) were densely immobilized on the surface of Au/SiO_2 particles (Au size: 13 nm). Figure 2 shows the photocatalytic H_2 evolution rate of $(AgIn)_xZn_{2(1-x)}S_2$ nanoparticles and their nanocomposites with Au particles. The photocatalytic activity of $(AgIn)_xZn_{2(1-x)}S_2$ nanoparticles was enhanced by the immobilization on the Au/SiO_2 particles. Furthermore the degree of the enhancement was different depending on the chemical composition of $(AgIn)_xZn_{2(1-x)}S_2$, in which the photoactivity of particles prepared with x=0.8 was much enlarged, probably due to the remarkable superimposition between absorption property of $(AgIn)_xZn_{2(1-x)}S_2$ nanoparticles and the LSPR peak of Au particles.

References 1) T. Torimoto, et al., *J. Phys. Chem. Lett.*, **2011**, 2, 2057. 2) T. Torimoto, et al., *J. Am. Chem. Soc.*, **2007**, 129, 12388.

M-P26-M

Fabrication of $L1_0$-FePd/α-Fe Nanocomposite Magnets from Compositionally Tuned Pd/γ-Fe_2O_3 Heterostructured Nanoparticles

K. Tada[1)*], R. Sato[1)] and T. Teranishi[1, 2)]
[1)]Faculty of Pure and Applied Sciences, University of Tsukuba, 1-1-1 Tennodai, Ibaraki 305-8571, Japan,
[2)]Institute for Chemical Research, Kyoto University, Gokasyou, Uji, Kyoto 611-0011, Japan
[*] k.tada@dmb.chem.tsukuba.ac.jp

Nanocomposite magnets (NCMs) consisting of hard and soft magnetic phases are one of candidate for overcoming the current theoretical limit of permanent magnet performance. Previously, we succeeded in fabrication of $L1_0$-FePd/α-Fe NCMs (magnetically hard $L1_0$-FePd and soft α-Fe phases). [1-2)] These NCMs had large $(BH)_{max}$ derived from the effect , whereas they are to show higher $(BH)_{max}$ value by controlling soft/hard volume ratios and aligning easy axis of magnetization. [3)] Here, we report the fabrication of $L1_0$-FePd/α-Fe NCMs with various soft/hard volume ratios by the reductive annealing of Pd/γ-Fe_2O_3 heterostructured nanoparticles (NPs).

Pd/γ-Fe_2O_3 heterostructured NPs were synthesized by the seed-mediated growth method. Figs. 1a-c show the TEM images of 8.2 ± 0.6 nm Pd seed NPs, Pd/γ-Fe_2O_3 NPs (Fe/Pd=3), and $L1_0$-FePd/α-Fe NCMs, respectively. We also succeeded in optimizing soft/hard volume ratios of $L1_0$-FePd/α-Fe NCMs . As a result, the sample with a hard/soft volume ratio of 75/25 had the largest maximum energy product (Fig. 1d, $(BH)_{max}$ = 7.3 MGOe). To further improve the $(BH)_{max}$ value, a synthesis of anisotropic NCMs will be also presented.

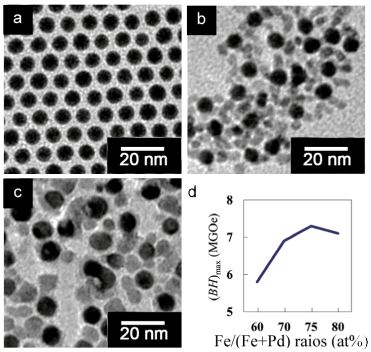

Fig. 1. TEM images of (a) 8.2±0.6 nm Pd seed NPs, (b) Pd/γ-Fe_2O_3 heterostructured NPs (Fe/Pd=3), and (c) $L1_0$-FePd/α-Fe NCMs (Fe/Pd =3). (d) $(BH)_{max}$ vs. Fe/(Fe+Pd) ratios for $L1_0$-FePd/α-Fe NCMs.

References : 1) T. Teranishi *et al*., *J. Am. Chem. Soc.* , 130, 4210-4211 (2008), 2) N. Sakuma, R. Sato. T. Teranishi *et al*., *ACS Nano.* 5, 2806-2814 (2011), 3) R. Skomski and J. M. D. Coey, *Phys. Rev. B*, 48, 15812-15816 (1993).

M-P02-M

Fabrication of Organic Semiconductor-based Nanowires and its Photovoltaic Applications by Single Particle Nanofabrication Technique (SPNT)

Y. Maeyoshi,[1)] A. Asano,[1)] H. Marui,[1)] M. Omichi,[1)] S. Tsukuda,[2)] M. Sugimoto,[3)] A. Saeki,[1)] and S. Seki[*1)]
[1)]Division of Applied Chemistry, Graduate School of Engineering, Osaka University, Suita, Osaka, Japan, [2)]Institute of Multidisciplinary Research for Advanced Materials, Tohoku University, Sendai, Miyagi, Japan, [3)]Takasaki Advanced Radiation Research Institute, Japan Atomic Energy Agency, Takasaki, Gunma, Japan.
[*]seki@chem.eng.osaka-u.ac.jp

High energy particles penetrating into polymeric materials give their kinetic energy to a limited nm-sized spatial area along their trajectories, leading to insoluble nanogels (nanowires) via cross-linking of the polymers. Nanowires are isolated on the substrate by the subsequent development procedures, and visualized clearly by an atomic force microscope.[1] The methodology; Single Particle Nanofabrication Technique (SPNT) is applicable to miniaturization of a variety of polymeric materials.[1-3]

In the present paper, we demonstrate the direct formation of nanowires consisting of semiconducting polymers and fullerene derivatives by SPNT. Poly(9,9'-dioctylfluorene) (PFO), regioregular poly(3-hexylthiophene) (rrP3HT), and poly[2-methoxy-5-(2'-ethylhexyloxy)-1,4-phenylenevinylene] (MEH-PPV) caused efficient cross-linking reaction upon particle irradiation, resulting in the successful fabrication of the nanostructures by SPNT (Figure 1a-c). The representatives of n-type small molecules: fullerene and [6, 6]-phenyl C_{61} butyric acid methyl ester (PCBM) were also found to give rod-like uniform nanowires with extremely small size distribution by SPNT (Figure 1d). With an use of a bi-layer film consisting of PFO (upper) and PCBM (lower), nanowires with p/n heterojunctions were successfully produced by SPNT. Moreover, aiming at the improvement of the power conversion efficiency of organic photovoltaic cell (OPVs),[4] we also fabricated bulk heterojunction OPVc based on nanowires of rrP3HT and PCBM as an active layer.

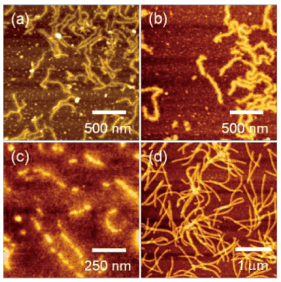

Fig. 1. AFM images of organic semiconductor-based nanowires produced by SPNT. Images (a) – (d) were observed in the thin films of PFO, rrP3HT, MEH-PPV, and PCBM after irradiation of 450 MeV Xe particles at the fluence of 1.0 ~ 3.0×10^9 ions cm^{-2}, respectively.

References : 1) S. Seki, *et al*., *Adv. Mater*., 13, 1663-1665 (2001)., 2) S. Tsukuda, *et al*., *Jpn. J.Appl. Phys*., 44, 5839-5842 (2005)., 3) S. Tsukuda, *et al*., *J. Phys. Chem. B*, 110, 19319-19322 (2006)., 4) A. Saeki, *et al*., *Adv. Energy Mater*., 1, 661-669 (2011).

M-22-M

Synthesis of Grid-type Fe_4 Spin-Crossover Cluster and Photo Magnetic Response Based on Intra-Molecular Magnetic Interaction

K. Miyahara[1)], S. Kanegawa[2)], S. Kang[2)] and O. Sato[*2)]

1) Interdisciplinary Graduate School of Engineering Sciences, Kyushu University, 6-1 Kasuga-koen, Kasuga, Fukuoka 816-8580, Japan

2) Institute for Materials Chemistry and Engineering, Kyushu University, 6-1 Kasuga-koen, Kasuga, Fukuoka 816-8580, Japan

*sato@cm.kyushu-u.ac.jp

Metal complexes exhibiting spin-crossover (SCO) induced by external stimuli such as light and temperature are great interest in the field of materials science. They have potential as components of magnetic storage devices. We have focused on a grid-type Fe(II) SCO tetra-nuclear cluster (**Fe_4**) that exhibits two-step decrease in magnetization due to spin transition and anti-ferromagnetic interacion.[1)] The metal ions in the cluster with square structure are bridged by oxygen atoms, in which intra-molecular elastic-, magnetic- and electric-interactions between metal ions operate. Hence it is expected that the **Fe_4** shows characteristic magnetic properties such as multi-step spin transition behavior and magnetic bistability.

In this study, we aimed at developing a cluster that shows cooperative SCO behaviors and intra-molecular magnetic interactions. The new **Fe_4** ($[Fe_4(\mathbf{H_1L_1})_4](BF_4)_4$: **1**) was synthesized by using a ligand (**$\mathbf{H_2L_1}$**) shown in Fig. 1. The magnetic properties were measured by SQUID as shown in inset of Fig. 2. Magnetic behavior suggests that **1** synthesized from ethanol has *trans*-type half high spin state (4LS⇔2HS-2LS⇔4HS). Photo magnetic response of **1** exhibited that magnetic susceptibility decreases by photo irradiation at $\lambda = 532$ nm below 25 K (Fig. 2). This means that intra-molecular anti-ferromagnetic interaction couples to spin transition in the tetra-nuclear cluster.

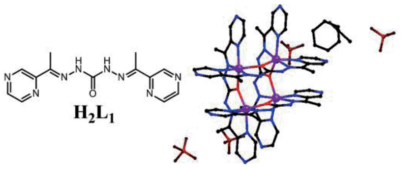

Fig. 1, Ligand (**$\mathbf{H_2L_1}$**), Crystal structure of **1**

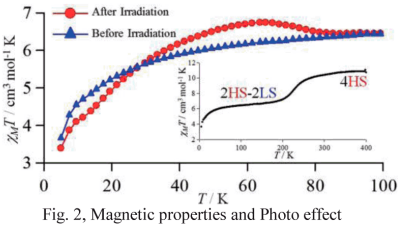

Fig. 2, Magnetic properties and Photo effect

1) D-Y.Wu, O.Sato, Y.Einaga, C-Y.Duan, *Angew. Chem. Int. Ed.*, **2009**, *48*, 1475-1478.

M-P21-D

Fabrication of Polystyrene Nanowires by the Single Particle Nano-Fabrication Technique

A. Asano[1)], Y. Maeyoshi[1)], S. Tsukuda[2)], M. Sugimoto[3)], H. Marui[1)], M. Omichi[1)], A. Saeki[1,4)], and S. Seki[1)*]

[1)]Department of Applied Chemistry, Graduate School of Engineering, Osaka Univ., 2-1 Yamada-oka, Suita 565-0871, Japan, [2)]Institute of Multidisciplinary Research for Advanced Materials, Tohoku Univ., 2-1-1Katahira, Aoba-ku, Sendai 980-8577, Japan, [3)]Japan Atomic Energy Research, 1233 Watanuki-machi, Takasaki, Gunma 370-1292, Japan, [4)]JST-PRESTO, Japan.

*seki@chem.eng.osaka-u.ac.jp

Radiation promotes various chemical effects in materials. In the case of polymeric materials, the major effects of radiation depend strongly on the relative efficiency of chain scission and cross-linking reactions. We have produced successfully 1-D nanostructures based on the cross-linking reactions in the thin films of several kinds of polymers by irradiation of high energy charged particles; single particle nano-fabrication technique (SPNT).

The fabrication of nanowires composed of acetylene-functionalized polystyrene (PSES) were confirmed by atomic force microscopy. PSES showed higher value of cross-linking efficiency than unsubstituted polystyrene. This result shows that acetylene groups promoted the cross-linking reaction. PSES nanowires were easily controlled the orientation and the aggregation structure by development procedures, respectively. It is well known that terminal alkyne groups can react with azide groups under Cu catalyst as click reaction, leading to effective surface modification via the functional groups. The height of nanowires was increased after modification of proteins. This result indicates that alkyne groups on the surface of nanowires maintain its function.

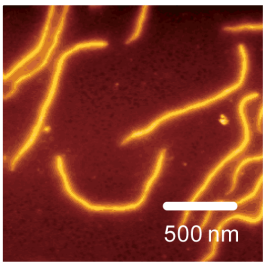

Figure. An AFM micrograph of nanowires based on PSES film prepared under exposing films to a 450 MeV $^{129}Xe^{23+}$ particles at 3.0×10^8 ions cm^{-2}.

References: 1) S. Seki *et al.*, *Adv. Mater.*,**13** (2001) 1663. 2) S. Seki, *et al.*, *Phys. Rev. B*, **70** (2004) 144203.

M-06-D

Platonic Hexahedron Composed to Six Organic Faces with an Inscribed Au Cluster

D. Tanaka*, M. Sakamoto and T. Teranishi[1,2]
[1] Faculty of Pure and Applied Sciences, Univ. Tsukuba & CREST-JST, 1-1-1 Tennodai, Tsukuba, Ibaraki 305-8571, Japan,
[2] Institute for Chemical Research, Kyoto University, Gokasho, Uji, Kyoto, 611-0011, Japan, *tanaka-d@dmb.chem.tsukuba.ac.jp

The structure of nanomaterial determines their individual properties and suprastructures they can form. Therefore, it is very important to crate the highly symmetric and size controlled nanostructure. In this study, we succeeded to synthesis nano Platonic hexahedron composed by spherical Au clusters (AuCs) and six porphyrins derivatives through the face-coordination of porphyrin derivatives on the AuC.

Three porphyrin derivatives (SC_nP, Fig.1), which have four acethylthio groups in the same direction against porphyrin ring were synthesized.[1] TEM observation revealed that Au clusters coordinated by these porphyrin derivatives (SC_nP-AuC) were about 1.2 nm in diameter. The MALDI-TOF-MS and ICP-AES measurements indicated that the composition of SC_nP-AuC were $Au_{\sim 65}(SC_1P)_{\sim 6}$ and $Au_{\sim 65}(SC_2P)_{\sim 6}$, respectively. Soret band absorption of SC_nP on AuC decreased depending on the distance between the AuC and porphyrin ring, infering the strong interaction between AuC and SC_nP (Fig.3).[2] There AuCs could be applied to various nanoelectronics like single electron transistor.[3]

References : 1) Kanehara, M.; Takahashi, H.; Teranishi, T. *Angew. Chem., Int. Ed.* **2008**, *47*, 307, 2) M. Sakamoto, D. Tanaka, T. Teranishi *et al.*, submitted, 3) Teranishi, T.; Majima, Y. *et al.*, *Appl. Phys. Exp.* **2010**, *3*, 105003.

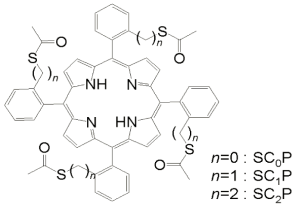

Fig.1 Structure of SC_nP.

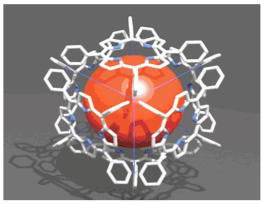
Fig.2 Schematic of SC_1P-AuC.

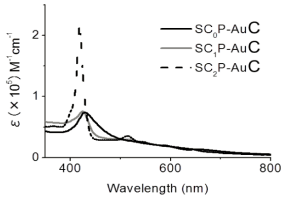

Fig.3 Absorption spectra of SC_nP-AuC.

Session N

N-P28-M

Effects of Water Soluble Wool Keratin on the Bleaching and Permanent Waving Treatments of Hair

R. Yuasa*, Y. Hirata, M. Takigami, Y. Tomita[1], M. Amaya[1] and S. Takigami
Graduate School of Engineering, Gunma University, 1-5-1 Tenjincho, Kiryu, Gunma 376-8515, Japan
1) Nicca Chemical Co. Ltd, 4-23-1 Bunkyo, Fukui, Fukui 910-8670, Japan
*t11801007@gunma-u.ac.jp

Coloring and permanent waving treatments cause some problems on hair. As hair has many similarities to wool, we used water soluble wool keratin, carboxymethylalanyl disulfide keratin (CMADK), to treat hair and studied effect of CMADK on damaged hair. Bleaching (B), permanent waving (P), bleaching and permanent waving (B&P) treatments have been done up to 3 times on virgin Japanese human hair. B&P in the presence of CMADK (BPW) was also carried out. The properties of treated hairs were investigated by a scanning electron microscope (SEM), an atomic force microscope (AFM), and an extensometer. Efficiency of permanent waving treatment was evaluated by visual observation of the shape, i.e., number of wave, space between waves, lengths of hairs before and after treatment.

Damage of cuticle was observed in B&P hair treated for 3 times, while cuticle layers were not damaged in BPW hair. CMADK was effective to prevent damage in cuticle layers by B&P treatment.

Elastic modulus and stress at yield point of treated hair were smaller than those of untreated hair. However, the decrease was smaller in BPW hair than that in B&P hair.

Photograph of hairs after permanent waving treatments without and with CMADK is shown in the figure. The number of wave was more in hair treated with CMADK than that in hair treated only with reductant.

The results described above suggested that CMADK is effective to reduce damage in B&P treated hair.

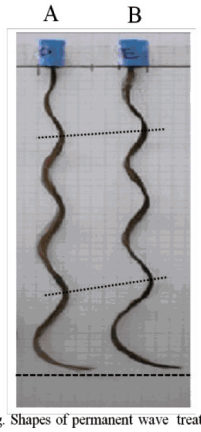

Fig. Shapes of permanent wave treated hair without and with CMADK.
A: Without CMADK
B: With CMADK 0.5%

N-P23-D

Efficient Antibacterial Action for Plant Powder in the Presence of Magnesium Oxide

K. Kurita*, H. Noda[1] and H. Iizuka[1]
Graduate School of Science and Engineering, Yamagata University [1]
*h4_k_rx7@yahoo.co.jp

Introduction

We found, recently, that a synergy effect on an antibacterial action for green tea ingredients in the presence of magnesium oxide (MgO). [1] This phenomenon was caused by hydrogen peroxide produced after the reaction between catechine in green tea and MgO. In this research, we have investigated the synergy effect on antibacterial action for some Plant powders except for green tea in the presence of MgO.

Method

Powdery sample of plants such as *phellodendron amurense*, *Rosmarinus officinalis* L., and green tea was prepared by clashing dry plants. MgO (0.01 μm, 99.9%) was purchased by Wako pure chemical industries, Ltd. A temporarily antibacterial property determination system was constructed with a sample, 1% polypepton solutions, and a desiccator having about 5L. An antibacterial effect was estimated by the measurements of CO_2, mercaptan, and ammonia production by using a gas-detecting tube.

Results and Discussion

The synergy effect on antibacterial action was observed from the cases of *phellodendron amurense* and *Rosmarinus officinalis* L. The synergy effect on the case of *rosmarinus officinalis* L. was the same amplitude as that of green tea. Our results, therefore, will give a useful antibacterial material for the organic farming.

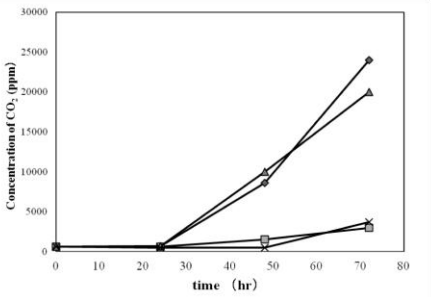

Fig. 1. CO_2 production of the systems in the presence of MgO(◇), *phellodendron amurense*/MgO(△), *Rosmarinus officinalis* L./MgO(□), and green tea/MgO(×).

References : 1) H. Noda, Y. Miyamoto, Koukinnzai, Patent No. 4202493, Japan, 17/10/ 2008.

Session O

O-09-M

Hydrothermal synthesis of hydrogarnet as the adsorbents for humic substances

Y. Kurosaki[1], H. Maeda[2], H. Ishida*[1] and Y. Suto[1]
[1] Tohoku University, 6-6-20 Aramakiaza-Aoba, Aoba-ku, Sendai 980-8579, Japan, [2] Nagoya Inst. of Technology, Gokiso-cho, Showa-ku, Nagoya 466-8555, Japan, *emile.h.ishida@mail.kankyo.tohoku.ac.jp

Humic substances generate carcinogens by reacting with chlorine, they are highly expected to be removed from aquatic environment. Humic substances have various structures and molecular weight. Therefore, adsorbents are required to have multiple adsorption sites rather than single composition. Previous studies reported that mesopores of activated carbon exhibit high adsorption properties however high temperature (>900 °C) is needed for invigoration. Hydrogarnet series $Ca_3Al_2(SiO_4)_{3-x}(OH)_{4x}$ [x=0-3] are continuous solid solution synthesized by hydrothermal treatment at temperatures less than 200 °C and consist of abundant elements on the earth. Electron density between the constituent atoms of hydrogarnet varies depending on silicon substitution contents. So, if hydrogarnet has gradient compositions, the various adsorption sites would appear and it's expected as the new adsorbent materials for humic substances. It has been reported that the silicon substitution contents vary with starting materials and temperature. In contrast, it's difficult to control the silicon substitution contents because of miscibility gap (x=2.24-2.58)[1]. In this study, we added alkali metal hydroxide into solvents in order to control the supersaturation for hydrogarnet.

Fig. 1 shows XRD patterns of the samples synthesized by hydrothermal treatment for 10-1440min using sodium hydroxide solution (0.1 M). There are peaks of $Ca_3Al_2(SiO_4)_{0.34}(OH)_{10.64}$ [x=2.66] and $Ca_3Al_2(SiO_4)_{0.22}(OH)_{8.88}$ [x=2.22] in 10minuts and $Ca_3Al_2(SiO_4)_{0.22}(OH)_{11.12}$ [x=2.78], $Ca_3Al_2(SiO_4)_{0.51}(OH)_{9.96}$ [x=2.49] and $Ca_3Al_2(SiO_4)_{1.38}(OH)_{7.32}$ [x=1.83] in 30minuts. We succeeded to synthesize three silicon substitution contents in same time including the composition of miscibility gap.

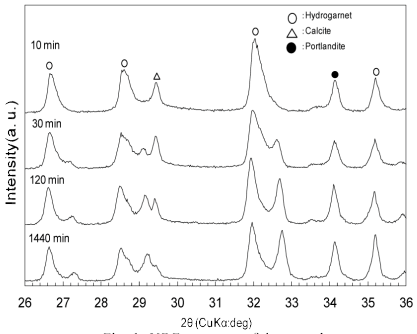

Fig. 1. XRD patterns of the samples.

1) T. G. Jappy, F. P. Glasser, *Advances in Cement Research*, Vol.4, pp.1-8 (1991)

Session P

P-06-G

Smart Shape-memory Surfaces for Mechano-structual Control of Cell Function

M. Ebara*, K. Uto, N. Idota, J. M. Hoffman, G. Forte, and T. Aoyagi
Smart Biomaterials Group, Biomaterials Unit, MANA Nano-bio field, National Institute for Materials Science (NIMS)
1-1 Namiki, Tsukuba, Ibaraki 305-0044 JAPAN.
*EBARA.Mitsuhiro@nims.go.jp

Shape-memory surfaces (SMSs) with on demand, tunable nano-patterns have been developed to observe time dependent changes in cell alignment using temperature-responsive poly(ε-caprolactone) (PCL) films. The PCL films were prepared by crosslinking tetra-branched and linear PCLs, each with acrylate end-groups. The critical temperature for temporary shape fixing and permanent shape recovery was controlled using branched PCL nano architectures only, without adding any other components. Permanent surface patterns were generated by crosslinking the PCLs in a mold. Temporary surface patterns were later embossed into the crosslinked SMSs. The application of body heat quickly and completely transitioned temporary surface patterns to permanent patterns. To observe the effects of a shape-memory-activated change in surface topography on cell behavior, surfaces with a temporary grooved pattern were used as a cell culture substrates and subsequently triggered to revert to a permanent flat surface in the presence of growing cells. A time-dependent decrease in cell alignment was observed as a result of remodeling of the actin cytoskeleton. Dynamically tunable nano-structured surfaces, therefore, can be used to study the effects of surface nano-geometries on time-dependent cytoskeleton remodeling under biological relevant conditions.

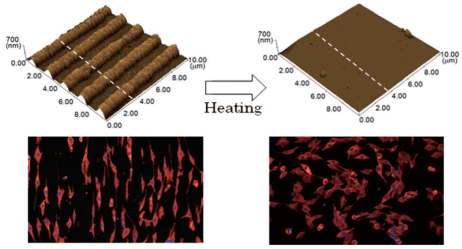

Fig. 1. Topographic surface images of PCL films observed by atomic force microscopy (AFM) and fluorescent microscope images of NIH 3T3 fibroblasts seeded on the PCL films before and after shape-memory transition by a 37C heat treatment.

References: 1) M. Ebara, K. Uto, N. Idota, J. M. Hoffman, T. Aoyagi, *Adv. Mater*, in press. 2) M. Ebara, J. M. Hoffman, A. S. Hoffman, P. S. Stayton, *Lab Chip*, 6, p. 843, 2006. 3) K. Uto, K. Yamamoto, S. Hirase, T. Aoyagi, *J. Contr. Rel.*, 110, p. 408, 2006.

P-15-D

One-step synthesis of mutant protein library on an ultralarge-scale integrated DNA microarray chip for high-speed molecular evolution

S. Sato[1)2)*], M. Biyani[1)3)], T.Akagi[1)3)] and T. Ichiki[1)3)]
[1)]School of Engineering, The University of Tokyo, 2-11-16, Yayoi, Bunkyo-ku, Tokyo, 113-8656, Japan, [2)]Center for Medical System Innovation, 2-11-16, Yayoi, Bunkyo-ku, Tokyo, 113-8656, Japan, [3)]Core Research of Evolutional Science and Technology, JST, 4-5-3, Chiyoda-ku, Tokyo 102-0075, Japan
*shusuke@bionano.t.u-tokyo.ac.jp

In the field of high-speed molecular evolution technology, high-throughput protein screening is a challenging issue and the use of microarray chip is one of the most promising approaches [1]. We have been developing a high-throughput protein synthesis and screening system based on ultralarge-scale microreactor array technology [2]. In this paper, we report the development of a simple and robust on-chip technology for the synthesis of mutant protein libraries.

The model DNA library employed in this study included a random sequence in 1 codon of a GFP (green fluorescence protein) chromophore region. Firstly, a DNA molecule (861 bp) from the library was amplified and immobilized on a magnetic bead (1.0 μm in diameter) using the BEAMing method [3]. Secondly, DNA-bound magnetic beads were self-organized into a high-density microreactor array (1.5 μm in diameter, 1.5 μm in height, 1.44×10^8 well/chip) using the assistance of an external dynamic magnetic force. Finally, an aqueous solution including the cell-free translation system and synthetic oil was sequentially poured onto the microreactor array chip to cover its entire surface. After incubation for 120 min at 30°C, mutant GFPs synthesized in the microreactors were successfully observed under a confocal microscope. We observed the different GFP fluorescence signals with respect to the microreactors (Fig. 1).

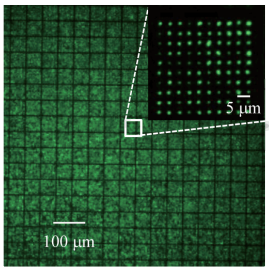

Fig.1 Microphotograph of mutant GFP library synthesized on a chip. Mutant GFPs were synthesized in a femtliter volume using cell-free translation system.

References : 1) A. Q. Emili, *et al.*, *Nature biotechnology*, 18, 393 (2000). 2) M. Biyani *et al.*, *14th ICMChemical*, (2010). 3) D. Dressman, *et al.*, *PNAS*, 100, 8817 (2003).

P-16-D

Localized Illumination in Polymeric Nanoholes for Single-molecule Imaging

T. Ono[*1, 2, 3)], R. Iizuka[3, 4)], T. Akagi[1, 3)], T. Funatsu[3, 4)] and T. Ichiki[1, 3)]
[1)] Grad. Sch. Eng., Univ. Tokyo, 2-11-16 Yayoi, Bunkyo-ku, Tokyo, [2)] Research fellow, JSPS, 8 Ichibancho, Chiyoda-ku,Tokyo,
[3)] CREST, JST, 5 Sanban-cho, Chiyoda-ku, Tokyo, [4)] Grad. Sch. Phar., Univ. Tokyo, 7-3-1 Hongo, Bunkyo-ku, Tokyo
[*]ono@bionano.t.u-tokyo.ac.jp

Localized illumination is an effective approach for high contrast ratio due to reduction of background noise. It allows single-molecule imaging which promise to elucidate biochemical reaction mechanisms. Total internal reflection fluorescent microscope (TIRFM) is a conventional method for the illumination. However, it has some limitations; firstly background noise becomes excessive in high fluorophore concentration because the illumination region is limited only vertically, and secondly the condition for total reflection is easily disrupted by device structure employed on TIRFM. Meanwhile, zero-mode waveguide (ZMW), an illumination device with metal nanoholes, further confines background noise more than TIRFM but it has also some issues, such as the nonradiative damping of fluorophore due to electron energy transfer to surface plasmon polariton of the metal. [1]

A new nanohole device we developed uses an amorphous perfluoropolymer, Cytop™ (Asahi Glass Co., Ltd.), and maintains the condition for total reflection because of the polymer's refractive index similar to that of water (1.34). It localizes its illumination volume three-dimensionally with the nanohole and TIRFM. Moreover, the device eliminates electromagnetic interaction.

The device was fabricated by thermal nanoimprint, oxygen plasma etching of thin residual layer and polyethylene glycol (PEG) modification for reduction of nonspecific adsorption. During SF_6/O_2 mixture plasma etching, silicon nanomold was cooled at -130ºC which is lower temperature than ordinary cryo-etching for anisotropic etched features (Fig. 1(a)). SEM image of the fabricated nanohole is shown in Fig. 1(b). After filled by water solution, the nanoholes confines excitation volume at their bottom (Fig.1(c)).

Reference [1] I. Pockrand *et. al.*, *Chem. Phys. Letters*, 69, 499-504 (1980).

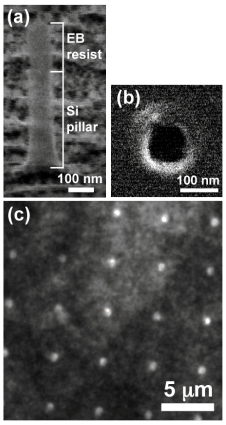

Fig. 1 Polymeric nanoholes for localized illumination. SEM images of (a)the nanomold and (b) nanohole (φ100 nm, 200 nm depth), and (c)Fluorescent image of 200 nM Cy5 in the nanoholes.

P-17-M

PLIC-VOF simulation of flow-assisted auto-dispensing of aqueous solution into a microreactor array

T. Fujita[1], M.Biyani[1,2] and T. Ichiki[1,2]
[1]Department of Bioengineering, School of Engineering, The University of Tokyo, JAPAN
[2]Core Research of Evolutional Science and Technology, Japan Science and Technology Agency, JAPAN
fujita@bionano.t.u-tokyo.ac.jp

Handling multiple droplets is a fundamental technology in high-throughput bio-analysis/synthesis. In the microtiter plate format, robotic dispensors are commonly used to enhance the rate and quality of liquid handling. On the other hand, self-assembly solution positioning by the hydrophobic-hydrophilic interaction can be used as another dispenser-free approach especially for a microreactor array with the volume smaller than nanoliter. We investigated oil flow-assisted auto-dispensing of aqueous liquid into microreactor array with the sub-femto-liter volume by numerical simulation using the piecewise linear interface construction-volume of fluid (PLIC-VOF) method.

The numerical simulation was performed using a multi-physics software package CFD-ACE+ (CFD Research Corporation). The microreactor array had 6 reactors (diameter: 4 μm, depth: 4 μm) in the length direction and was infinite in the width direction on planar channel (height; 12 μm, length; 40 μm) with 4 μm pitch. The channel and microreactors were initially filled with water. The pressure of 30 kN/m^2 was applied at the inlet. The dynamic contact angle at the water-oil-solid interfaces was set at 170±10°.

Figure 1 (a) shows a typical snapshot of the simulation result. One-directional oil flow with the velocity of 0.26 m/s sequentially dispensed water into the arrayed microreactors and formed spherical water-oil ceiling. Fig. 1 (b) shows the average time is 27 μs to seal each reactors. The viscous friction at water-oil interface caused vortex flow (maximum velocity; 0.25±5 m/s) in the water phase of each microreactors as shown in Fig.1 (c). The volume of sealed water was 39.5±2 atto liter (78±4 % of reactor volume).

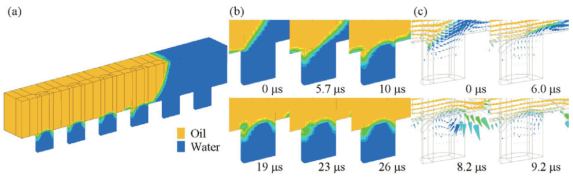

Fig.1 (a) A snapshot of sealing water into the microreactor array using oil flow. (b) Time evolution of sealing water into a microreactor. (c) Flow velocity distribution around a microreactor.

P-P29-G

Suppression of thermal inactivation of proteins by solution additives.

S. Tomita[1)], Y. Nagasaki[1-3)], K. Shiraki[*1)]
[1)] Grad. Sch. of Pure and Applied Sci., Univ. of Tsukuba, 1-1-1 Tennodai, Tsukuba, Ibaraki 305-8573, Japan. [2)] Grad. Sch. of Comprehensive Human Sci., Univ. of Tsukuba, 1-1-1 Tennodai, Tsukuba, Ibaraki 305-8577, Japan. [3)] MANA, NIMS, 1-1-1 Tennodai, Tsukuba, Ibaraki 305-8577, Japan. *shiraki@bk.tsukuba.ac.jp

Proteins tend to undergo irreversible inactivation through several chemical modifications, which is a serious problem in various fields. It is known that irreversible thermoinactivation of bovine pancreatic ribonuclease A (RNase A) and hen egg white lysozyme at neutral pH is caused by a combination of a few well-defined reactions: deamidation of asparagine (Asn) residues, destruction of disulfide bonds through β-elimination, and the formation of incorrect structures through disulfide interchange [1]. Based on this fact, we investigated the effects of various solution additives on the thermal inactivation of both proteins. Firstly, it has been shown that several kinds of low-MW solution additives, such as arginine (Arg), amidated amino acids, and polyamines, suppress thermal deamidation and β-elimination of proteins, resulting in the suppression of thermal inactivation [2]. Secondly, we have found that poly(ethylene glycol) (PEG) with MW higher than 1000 highly inhibit intermolecular disulfide interchange, presumably due to the inhibition of intermolecular collision of thermally denatured proteins [3]. Therefore, it should be pointed out that the mechanism of action between low-MW solution additives and PEG on the suppression of thermal inactivation of proteins is clearly different. Accumulation of knowledge about solution additives that control stability of proteins would enable researchers to rationally design the appropriate solution conditions for each protein.

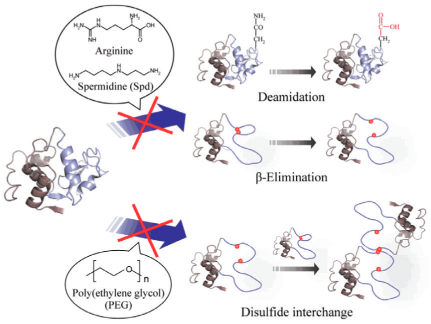

Fig. 1. A schematic illustration of the mechanism of solution additives on the thermal inactivation of proteins.

References: 1) T.J. Ahern, A.M. Klibanov, *Methods Biochem. Anal.*, 33, 91-127 (1988), 2) S. Tomita, K. Shiraki, *Biotechnol. Prog.*, 27, 855–862 (2011), 3) S. Tomita, Y. Nagasaki, K. Shiraki, *In preparation*

P-P54-D

Boron Neutron Capture Therapy Assisted by Nanoparticles: Enhanced Tumor Accumulation by core-polymerization with boron-containing monomer

Shogo Sumitani[1], Tatsuya Yaguchi[1], Hiroki Murotani[1], Yukichi Horiguchi[1], Minoru Suzuki[4], Koji Ono[4], Hironobu Yanagie[5], Yukio Nagasaki[1-3]
[1]Graduate School of Pure and Applied Sciences, [2]Graduate School of Comprehensive Human Sciences, University of Tsukuba, [3]MANA NIMS, [4]Radiation Oncology Research Laboratory, Research Reactor Institute, Kyoto University, Osaka, [5]Department of Nuclear Engineering and Management, School of Engineering, University of Tokyo.
s-sumitani@ims.tsukuba.ac.jp

Boron neutron capture therapy (BNCT) has attracted much attention as the selective and noninvasive cancer therapy using ^{10}B compounds, which efficiently generate the cytotoxic α-particles and ^{7}Li nuclei within ten μm through the nuclear reaction of ^{10}B atom with low-energy thermal neutrons. The success of BNCT is dependent on the delivery systems to accumulate a sufficient quantity of ^{10}B to tumor tissues. In this study, we designed and prepared core polymerized micelles (PM micelles) composed of poly(ethylene glycol)-*block*-poly(lactide) copolymer bearing an acetal group at PEG end and a methacryloyl group at PLA end (acetal-PEG-*b*-PLA-MA) and polymerizable boron cluster (1-(4-vinylbenzyl-*closo*-carborane): VB-carborane). The PM micelle proved to prolong the blood circulation time and deliver the ^{10}B to the tumor tissues without release of boron clusters in the blood stream compared to non polymerized micelles (NPM micelles) because of the existence of covalent bonds between VB-carborane and the PLA core of the micelles. Neutrons irradiation was carried out at the JRR4 and KUR. ^{10}B-enriched PM and NPM micelles were injected into colon-26 tumor bearing mice via the tail vein 24 h before irradiation. As comparison, ^{10}B-enriched sodium borocaptate (BSH; hydrophilic boron compounds) solution was injected 1 h before irradiation. **Fig. 1** shows the change in the tumor volume in mice treated with the irradiation of thermal neutrons. Note that the significant suppression of growth of tumor volume in mice injected with the ^{10}B-enriched PM micelles was observed from 12 days.

In conclusions, the PM micelles composed of acetal-PEG-*b*-PLA-MA and VB-carborane were prepared to suppress non-specific release of boron compounds in the blood stream. Worth noticing that the PM micelles showed remarkable therapeutic efficiency on BNCT; *viz*, selective and non-invasive BNCT was achieved. Therefore, the PM micelles represent a promising approach to the creation of novel boron carrier for cancer BNCT.

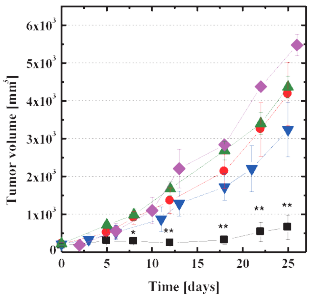

Fig. 1 Tumor growth curve of tumor-bearing mic injected the PM micelles (black squares) or the NPM micelles (red circles), normal saline (green triangles) 24 h before irradiation and BSH 1 h before irradiation (blue triangles). The PM micelles were injected into the mice without the irradiation (purple lozenges) as controls. The data are expressed as means ± S.E.M. (n = 5, *p<0.05, **p<0.01 against control at the same

P-P02-M

Microintaglio Printing Method for mRNA Fine Patterning

R. Kobayashi[1)*], Y. Tanaka[1)], S. Sato[1)], S.Ueno[2),3)], M.Biyani[1),2)] and T. Ichiki[1),2)]
Department of Bioengineering, School of Engineering, The University of Tokyo, 2-11-16, Yayoi, Bunkyo-ku, Tokyo, 113-8656, Japan[1)], JST/CREST, 5, Sanbancho, Chiyoda-ku, Tokyo 102-0075, Japan[2)], Department of Functional Material Science, Saitama University, 255 Shimo-okubo, Sakura-ku, Saitama-City, Saitama, 338-8570, JAPAN[3)]
[*]kobayashi.r@bionano.t.u-tokyo.ac.jp

High-throughput immobilization and precise micropatterning of biomolecules (e.g., nucleic acid (DNA/RNA), and proteins) onto a solid surface are crucial technologies for biodevices such as microarray chips. To overcome the essential limitation of conventional technologies such as spotting and microcontact printing, we have developed "microintaglio printing" method [1]. In this method, micropatterns are printed from the microengraved intaglio plate filled with biomolecular ink by means of pressure. In this presentation, we report the fine microintaglio printing of mRNA via hybridization with linker DNA on gold surface.

Firstly, the self-assembled monolayer (SAM) of DNA linker was formed on the sputter-coated gold film on the glass slide with an area of 20x20 mm^2 as follows. A 500 µl solution of 1 µM alkanethiol-modified oligonucleotide was dropped on the gold surface and incubated for 4 hours at room temperature, followed by the immersion in 1 mM 6-mercaptohexanol for 1 hour. The PDMS micromold plate with fine hole structures of 1.4 µm in diameter and depth was fabricated by soft lithography. After sandwiching a droplet containing of 500 pM mRNA of GFP (819base) synthesized with Cy5-labeled dUTP between a SAM DNA linker modified substrate and a micromold plate, hybridization was conducted under annealing condition (lowering the temperature linearly from 70ºC to room temperature). Figure 1 shows the fluorescence micrograph of mRNA dots patterned by microintaglio printing. A fine patterns of 1.4 µm in diameter were printed with the high selectivity since the biomolecular immobilization on the substrate was initiated after the tight contact of micromold by using the temperature control.

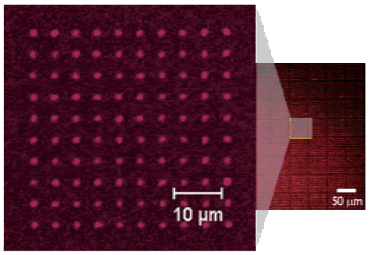

Fig.1 Fluorescent microscopic image of the mRNA array patterned by microintaglio printing.

Reference : [1] Biyani *et al.*, Appl. Phys. Express, 4 ,047001 (2011)

P-P16-M

Adhesion of biodegradable hydrogels utilizing the polyion complex formation through impressed voltage

W. Kawai, T. Asoh and A. Kikuchi*
Department of Materials Science and Technology, Tokyo University of Science, 2641 Yamazaki, Noda-shi, Chiba 278-8510, Japan, *kikuchia@rs.noda.tus.ac.jp

The development of microstructure regulated three dimensional (3-D) materials has attracted much attention in the field of tissue engineering. 3-D matrices with highly organized and stratified architectures composed of biodegradable and biocompatible polymers and/or cell-extracellular matrices (ECM) composites have been prepared. Adhesion of soft materials including hydrogels has therefore attracted attention because it is one of the most important processes for building functional soft constructs. However, the presence of solidified glues will limit the softness of adhesive coated surfaces and/or restrict mass transfer between two hydrogels. We recently reported a novel strategy for the adhesion of cationic and anionic stimuli-responsive hydrogels. [1] During electrophoresis, cationic and anionic polymers move to the cathode and anode, respectively. Then, polyions were diffused inside of the gels and adhesion was achieved through the formation of a polyion complex at the interface of the two hydrogels. The adhered hydrogels were quite stable in water during repetitive swelling and shrinking processes. Herein we report the adhesion of biodegradable hydrogels for building 3-D constructs *via* electrophoretic adhesion. Cationic and anionic gelatin based hydrogels showed unique adhesion characteristics as shown by ordered electric field application (**Fig. 1**). An increase in the electrophoresis time resulted in an increase in the adhesive strength of the two gels. Adhered gels were simply detached by applying an inverse electric field and the two gels re-adhered on the same surface when the electric field was reapplied. Moreover, electrophoretic adhesion of two hydrogels having the same charge was achieved using an oppositely-charged polymer as a binder.

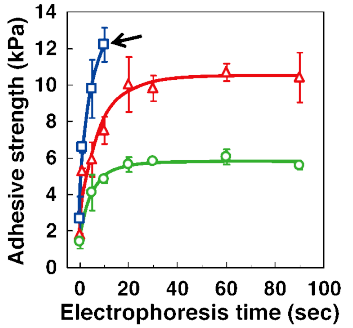

Fig. 1 Adhesive strength of adhered gelatin/PGA10 (circle), chitosan/PGA10 (triangle) and chitosan/PGA20 (square) gels as a function of electrophoresis time (n = 3). The arrow shows where the adhered gels have broken. Data are expressed as the mean ± standard deviation (S.D.).

In conclusion, we report on the electrophoretic adhesion of biodegradable hydrogels for building 3-D constructs. Electrophoretic adhesion will be useful in the field of tissue engineering for the development of 3-D soft materials with highly organized and stratified architectures composed of biodegradable and compatible polymer hydrogels.

References: 1) T. Asoh, A. Kikuchi *Chem. Commun*. **2010**, *46*, 7793-7795

Session Q

Q-P11-M

Multi-array formation of hepatocyte hetero-spheroids on micro-fabricated PEG-gel surface

S. Okimura[1)], M. Nagamura[1)], K. Sasaki[1)], S. Suzuki[2)] and H. Otsuka[1,*)]
[1)] Department of Applied Chemistry, Faculty of Science, Tokyo University of Science, 1-3 Kagurazaka, Shinjuku-ku, Tokyo 162-8601, Japan. [2)] Human & Animal Bridging Research Organization.
Phone: +81-3-5228-8265. Fax: +81-3-5228-8265. E-mail: *h.otsuka@rs.kagu.tus.ac.jp (Corresponding author).

Microarray technology allows the simultaneous analysis of thousands of parameters within a single experiment. Microspots of capture molecules are immobilized onto a solid support and exposed to samples containing the corresponding binding molecules. Such miniaturized and parallelized binding assays can be a useful tool to characterize gene and protein expression patterns in human disease processes in order to identify novel molecular targets for therapy.
Intensive investigation of proteins and chemical networks that comprise the cells and tissues of an organism, and the specific roles of proteins in these networks, will be a necessary next step to understand cellular functions in healthy and diseased states. Tissue and cell-based biosensors (TBB and CBB) will facilitate clinical and pharmaceutical analysis of molecular targets, because living cells can monitor the targets through their physiological changes that are induced by exposure to drugs and environmental perturbations, such as toxicants, pathogens or other agents. Hepatocytes are the most useful candidate to construct TBB and CBB. Spheroids are widely used in biology because they provide an in vitro 3-dimensional (3D) model to study proliferation, cell death, differentiation, and metabolism of cells in tumors and the response of tumors to radiotherapy and chemotherapy. The methods of generating spheroids are limited by size heterogeneity, long cultivation time, or mechanical accessibility for higher throughput fashion.
In this study, the micropatterning of hepatocyte hetero-spheroids underlaid with nonparenchymal feeder cells, exhibiting high viability and vigorous liver-specific function, was prepared on micro-fabricated glass substrates coated with poly(ethylene glycol) (PEG) gels. These arrayed spheroids as miniaturized liver may be highly useful for TBB, offering the promise of sensing drugs and environmental threats through a cellular physiological response. This technique is useful as a tool to obtain insights into the mechanism of cell-cell interaction, a central research topic in cell biology.

Q-P12-B

Phenylboronic acid functionalized polymer surface, exhibiting anomalous binding profile with N-acetylneuraminic acid (Neu5Ac)

Y.Maejima[1)], Y. Takahashi[1)], A. Matsumoto[2)], K. Kataoka[3)], Y. Miyahara[2)] and H. Otsuka[1,*)]
[1)] Department of Applied Chemistry, Faculty of Science, Tokyo University of Science, 1-3 Kagurazaka, Shinjuku-ku, Tokyo 162-8601, Japan. [2)] Tokyo medical and dental Univ. [3)] The Univ. of Tokyo.
Phone: +81-3-5228-8265. Fax: +81-3-5228-8265. E-mail: *h.otsuka@rs.kagu.tus.ac.jp (Corresponding author).

Borates are known to interact with carbohydrate moieties expressed on the surface of biological membranes of a variety of cells, viruses, bacteria, and fungi. This study revealed the anomalous binding profile of borate fuctionalized block copolymer tethered on surface with N-acetylneuraminic acid (Neu5Ac, sialic acid) as a potential receptor site on the surfaces of biological membranes. 3-amino phenylboronic acid (APBA) was chosen as the model borate compound. Usually, phenylboronic acid in water exists as an equilibrium mixture of the nonionic trigonal boronic form and the ionic tetrahedral monoborate form. (Scheme) It is known that the tetrahedral-formed phenylboronate can form significantly stable covalent bonds with polyol compounds including glucose in aqueous solution. On the other hand, complex of trigonal boronic acid is easy to hydrolyze, and can't exist stably in aqueous solution. Therefore, complexation equilibrium between boronic acid and polyol compounds could be controlled by pH change. In this study, the surface properties resulting from specific binding for Neu5Ac to APBA was compared with those for glucose, mannose, and galactose, which are the major carbohydrate constituents of glycoproteins and glycolipids expressed on biological membranes. In the Neu5Ac/APBA system, the unusual pH dependency of the binding, a decrease in binding with increasing pH, was observed, suggesting the formation of a trigonal-formed complex stabilized by the coordination of an amide group of Neu5Ac at the C-5 position to the boron atom. Furthermore, when boronic acids are used in biosystem, especially in human body, the binding/dissociation reaction with polyol compounds should be conducted at a constant pH under the physiological condition. Since the anomalously high complexing ability of PAPBA and Neu5Ac at physiological pH 7.4 was confirmed for this system, this exceptionally high binding character at physiological pH, compared to those of other sugars, strongly suggests that the boronic acid selectively recognizes the Neu5Ac residues of the glycosylated components including glycoproteins and gangliosides existing on the surface of the biological membranes.

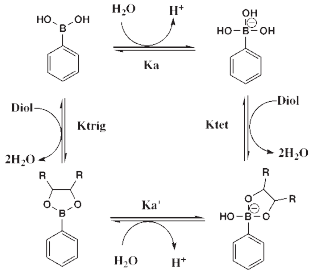

Session R

R-P09-B

Fabrication of chitosan/carbon micro coil composite membranes for bone tissue engineering

K.Bando[1)*], T.Aokage[2)], K. Tsuchiya[1)], and H. Yajima[1,2)]
[1)] Department of Applied Chem., Faculty of Sci., Tokyo Univ. of Sci.,[2)]Graduate School of Chem. Sci. and Tech., Tokyo Univ. of Sci.,1-3 Kagurazaka, Shinjuku-ku, Tokyo 162-8601, Japan, [*]yajima@rs.kagu.tus.ac.jp

In order to develop a newly efficient material for bone tissue engineering, we have intended to fabricate chitosan (Ch)/carbon micro coil (CMC) composite membranes, on which bone-like hydroxyapatite (HAp) is produced with simulated body fluids (SBF) to enhance boneconductivity of the material[1)]. Ch has been widely used in various biomedical applications due to its non-toxic and biodegradability[2)]. However, since Ch has poor cytocompatibility and apatite forming ability, the usage of Ch is prevented in tissue engineering. On the other hand, CMC with unique physicochemical properties was used as carbon material filler to Ch. CMC offers the possibility of a new magnetic sensor, and because of its particular 3D helical/spiral structure and characteristics, such as electromagnetic waves absorption and high hydrogen absorption. However, CMC has been not yet sufficiently studied with regard to the availability for biomaterials. The objective of this study is to improve the boneconductivity of Ch with CMC and SBF. CMC was blended into Ch solution (0.5 wt% and 5 wt%) and agitated by ultrasonication. CMC was oxidized with HNO_3/H_2SO_4 mixed acidic solution to enhance apatite forming ability. Ch/CMC composite films prepared by casting method were immersed in SBF for one week to form HAp on the films. SEM micrographs showed that the apatite forming ability of the composite film (0.5wt%) was considerably higher than that of the Ch film alone (Fig.1). Then, the attachment of osteoblast cells (MC3T3-E1) on the HAp-forming Ch/CMC films were observed by SEM, and their cell proliferation was performed by MTT assays. The number of spreading cells on the composite films was higher than that on the Ch film alone. The results obtained in the present study concluded that Ch/CMC films have possibilities to apply to efficient scaffolds for bone tissue engineering.

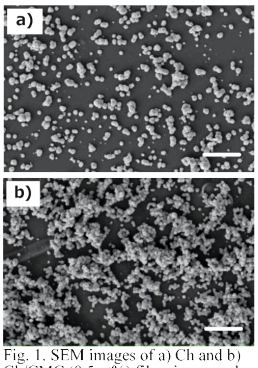

Fig. 1. SEM images of a) Ch and b) Ch/CMC (0.5wt%) films immersed inSBF.

References: 1) Dutta,et al.: Chitin and chitosan for versatile applications, J.Macromol.Sci .,42:307-354 (2002), 2) Tanahashi M,et al.: Apatite coating on organic polymers by a biomimetic process ,AM CERAM Soc., 77, 2805-8(1994)

R-22-G

Growth of Si sheet without cutting loss using substrate repelling Si melt

H. Itoh*, C. Nakamura, M. Mimura, M. Nobutoh, R. Komatsu
Yamaguchi University, Ube 755-8611, Yamaguchi, Japan
* ito-hrnr@yamaguchi-u.ac.jp

The photovoltaic power generation is one of the most promising renewable energy. At present, about 90% of solar cells were based on crystalline Si wafers. Undesirably, production of Si wafers for solar cells accompanies cutting process of Si ingots and more than 60% of Si ingots have been wasted as cutting loss [1]. If Si wafers were grown directly without cutting loss, the amount of wasted solar grade (> 6N) Si would drastically reduce and the cost of solar cell production could also be reduced. In this study, Si sheet crystal was grown using the substrate repelling Si melt.

The film consists of Si_3N_4, SiO_2 and organic particles were fabricated on AlN substrate by spin coating method. This substrate was fired at N_2 atmosphere after the removal of organic particles to make the film become porous ceramics. Si wafer with 0.8 mm thickness was sandwiched between two substrates which are vertically placed in the crucible. The vertical tube furnace was used for melting and crystal growth of Si. After the melting of Si, the crucible was moved to downward direction (20 mm/h) for the unidirectional solidification of Si. The surface of grown Si sheet was polished and etched by 10% NaOH solution for the observation of grain boundaries.

About 30×40×0.8 mm^3 sized multicrystalline Si sheet was successfully grown and the adhesion of Si with the substrates was not observed. Fig. 1 shows the grown Si sheet after polishing and etching. The undercooling of Si melt was supposed to be increased during the crystal growth because the average grain size of upper part is smaller than that of lower part. The crystal growth condition should be optimized by further study.

This study is supported by Regional Innovation Cluster Program (Global Type) by Ministry of Education, Culture, Sports, Science and Technology; Yamaguchi Green Materials Cluster (H21~H23).

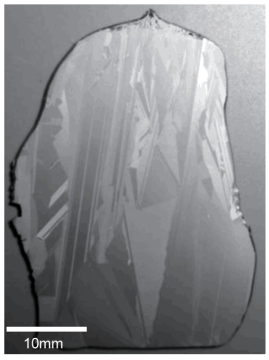

Fig. 1. Grown multicrystalline Si sheet after polishing and etching.

Reference; [1] D. Sarti and R.Einhaus: Solar Energy & Solar Cells 72 (2002) 27-40.

R-12-G

Carbon Membranes from Wood Materials and Their Separation Properties

T.Koga[1], Y.Takesue[1], T.Ikuta[1], Y.Imanami[1], K.Tanaka[1)], H.Kita[1)*], T. Suzuki[2)] and M.Funaoka[3)]
[1)]Yamaguchi University, Ube, Yamaguchi 755-8611, Japan, [2)]Kitami Institute of Technology, Kitami, Hokkaido 090-8507, Japan,
[3)]Mie University, Tsu, Mie 514-8507, Japan,
[*]kita@yamaguchi-u.ac.jp

Carbon membranes were prepared by coating thin layers of lignin or wood tar and then carbonizing by high frequency induction heating. In order to sustain the production of materials for human life under a sound ecological system, it is important to produce functional materials from renewable resources, and not from fossil resources. The permeation properties of the carbon membranes derived from the wood materials which have scarcely been utilized seem to be a promising candidates for the precursor materials of molecular sieving carbon membrane. The thickness of the membrane formed on the outer surface of a porous alumina substrate was less than 1000 nm judging from SEM observation (Fig.1). The carbon membranes show the molecular sieving property and have much higher performance than polymer membranes. Gas and water adsorption measurements indicated that carbon membranes have micropores in the range of 0.6-0.5 nm. C_{1s} peak of XPS spectra of the carbon membranes clearly showed that there are several hydrophilic functional groups, containing oxygen groups, on the surface of the membranes. Thus, the membrane showed water-selectivity in pervaporation system of water/alcohol. It can be concluded that carbon membranes from wood materials provide a promising new class of materials for the dehydration membranes for separation of water/alcohol.

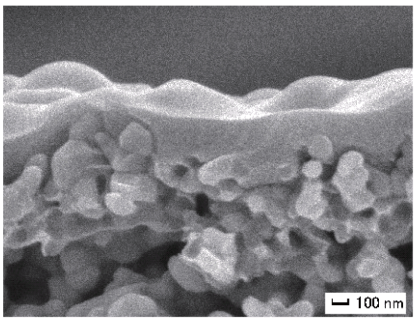

Fig.1 SEM view of the cross section of carbon membrane prepared from lignin at 600°C

Session S

S-12-G

Anhydrous Proton Conductivity of $KHSO_4$-$H_3PW_{12}O_{40}$ Composites and the Correlation with Hydrogen Bonding Distance under Ambient Pressure

S.Y. Oh[1,*)], T. Kikuchi[1)], Z.P. Li[2)], T. Mori[2)], G. Kawamura[1)], H. Muto[1)], and A. Matsuda[1,**)]
[1)]Department of Electrical and Electronic Information Engineering, Toyohashi University of Technology, Tempaku-cho, Toyohashi, Aichi 441-8580, Japan, [2)]Global Research Center for Environment and Energy based on Nanomaterials Science (GREEN), National Institute for Materials Science, Japan, [*]**so009@edu.imc.tut.ac.jp**, [**]**matsuda@ee.tut.ac.jp**

In this study, we focused on correlation between anhydrous proton conductivity and hydrogen bonding distance for $KHSO_4$-$H_3PW_{12}O_{40}$ (KHS-WPA) composites to clarify a design of new proton conductive electrolytes. Mechanochemical treatment was applied to the synthesis of high proton conductive composites. The mechanochemical treatment condition was the same as described in the previous report [1]. Composites with the ratio xKHS·(100-x)WPA were prepared, where x was varied between 50 and 95 mol%. From the ^{1}H-MAS-NMR spectra, the hydrogen bonding distance (L in pm) between KHS and WPA can be estimated using the relation $L = 100 \times (79.05 - \delta_{iso}) / 25.5$, where δ_{iso} is the highest ^{1}H chemical shift expressed in ppm with respect to the TMS signal.

Fig. 1 shows the relationship for xKHS·(100-x)WPA composites between L and anhydrous proton conductivity at 100 °C, i.e., much lower temperature than dehydration temperature (≈180 °C) of KHS. For the mechanochemically synthesized xKHS·(100-x)WPA composites, the anhydrous proton conductivity showed a good negative correlation with the hydrogen bond distance (O (H)···H). This observation indicated that anhydrous proton conductivity was significantly depending on hydrogen bonding and proton hopping distance, and implied that newly developed hydrogen bond was main role to improve anhydrous proton conductivity of composite rather than characteristic of hydrogen sulfates, namely independent of the presence of the superprotic phase [2].

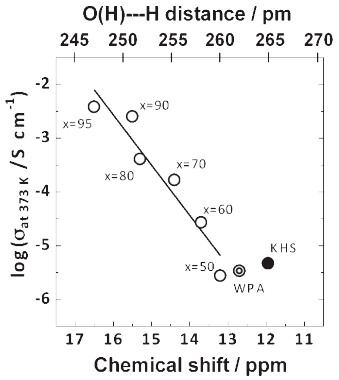

Fig. 1. Correlation between hydrogen bond distance (L) and anhydrous proton conductivity at 100 °C under ambient pressure for xKHS·(100-x)WPA composites.

1) A. Matsuda, T. Tezuka, Y. Nono, K. Tadanaga, T. Minami, and M. Tatsumisago, *Solid State Ionics*, 176, 2899-2904 (2005).
2) A. Matsuda, S. Y. Oh, V. H. Nguyen, Y. Daiko, G. Kawamura, H. Muto, Electrochim. Acta, 56, 9364-9369 (2011).

S-03-G

Electrical Conductivity Degradation of Ni-Doped Yttria-Stabilized Zirconia Electrolyte under SOFC Condition

T. Shimonosono*, H. Kishimoto, K. Yamaji, D.-H. Cho, F. Wang, M. Nishi, M.E. Brito, T. Horita, H. Yokokawa
National Institute of Advanced Industrial Science and Technology (AIST), AIST Central 5-2 1-1-1 Higashi, Tsukuba, Ibaraki 305-8565 Japan, *t-shimonosono@aist.go.jp

The 8%-yttria-stabilized zirconia (YSZ) which is the conventional electrolyte material of solid oxide fuel cells (SOFCs) undergoes cubic to tetragonal phase transformation accompanied with electrical conductivity degradation during annealing at 1273 K for ~1000 h[1]. Nickel doping of YSZ accelerated this phase transformation[2] and conductivity degradation in a reducing atomsphere[3]. Nickel probably diffuses into YSZ electrolyte during SOFCs fabrication process at high temperatures. We have observed phase transformation of stabilized zirconia of the electrolyte in regions near the anode; and for several real SOFCs stacks[4]. In this study, we have clarified the degree of the electrical conductivity degradation of Ni-doped YSZ electrolyte under SOFC condition, and investigated the effect of electrical loading. Figure 1 shows the variation of electrical conductivity and terminal voltage with time at 1173 K. At time of 0 h, the H_2 gas including 1 % H_2O was introduced to the anode side and the terminal voltage was increased close to the theoretical value. The degradation in conductivity of Ni-doped YSZ electrolyte was accelerated by exposure to humidified H_2 (closed circles) under OCV condition and reached 1/2 of initial value. Interestingly enough, the accelerated conductivity degradation was suppressed under the constant terminal voltage of 0.7 V (closed squares). Such effect of the electrical loading was attributed to the increase of oxygen partial pressure at the anode/electrolyte interface due to the overvoltage.

Acknowledgment : A part of this study was financially supported by NEDO of Japan. References : 1) K. Nomura et al., *Solid State Ionics*, 132, 235-39 (2000)., 2) A. Lefarth et al., *ECS Transactions*, 35 (1), 1581-86 (2011)., 3) W.G. Coors et al., *Solid State Ionics*, 180, 246-51 (2009)., 4) H. Kishimoto et al., *ECS Transactions*, 35 (1), 1171-76 (2011).

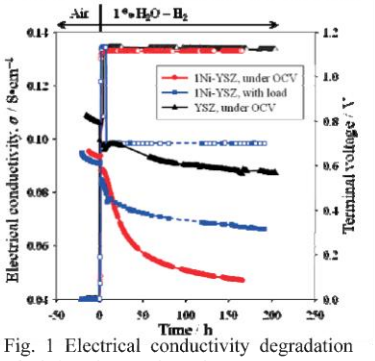

Fig. 1 Electrical conductivity degradation of Ni-doped YSZ electrolyte at 1173K

S-07-G

Preparation of Double Columnar Cathode Interface, $Ce_{0.8}Sr_{0.2}O_2$-$Sm_{0.5}Sr_{0.5}CoO_3$, with PLD Method for Improving Power Density Of the Cell Using $LaGaO_3$ Thin Film Electrolyte

J.W. Ju*, and T. Ishihara
Department of Applied Chemistry, Faculty of Engineering, Kyushu University, Motooka 744, Nishi-ku, Fukuoka, 819-0395, *ishihara@cstf.kyushu-u.ac.jp

Ni base cermet substrates have been popularly used as anode supporter. The cermet substrate such as NiFe-SDC anode shows a high power generation property due to large reaction area in 3-dimensional directions. However, the cermet substrates have insufficient mechanical strength. Therefore, at present, metal-supported SOFCs have been attracting much interest due to higher mechanical strength and thermal tolerance comparing ceramic-supported cells. In our previous work, we could confirm the Ni-Fe metallic anode supported cell exhibited the excellent power generation property at intermediated temperature. However, at lower temperature such as 773 and 673 K, the power density of the cell was still insufficient. From the analysis of internal resistance of the cell, it has confirmed the insufficient performance originated from increasing cathodic internal resistance. Therefore, in this study, we investigated deposition of columnar type cathode by PLD method and also applied for high power density SOFC at low temperature.

Figure 1 shows the power generation property of the cell having SSC-SDC double columnar cathode. Obviously, much higher power density is achieved by using double columnar electrode for cathode. In particular, at higher temperature, improvement in power density is much higher than the conventional cell and the maximum power density is as high as 2.2 W/cm^2 at 973K. This could be explained by the expanded reaction area by using oxide composite. However, at 673 K, the maximum power density was slightly decreased comparing with that of single SSC cone electrode. This may be related with decreased electrical conductivity of SSC-SDC composite. Therefore, by optimizing the composition, maximum power density at 673 K could be further improved and the power density of 160 mW/cm^2 was exhibited at 673 K, after optimizing double columnar composition.

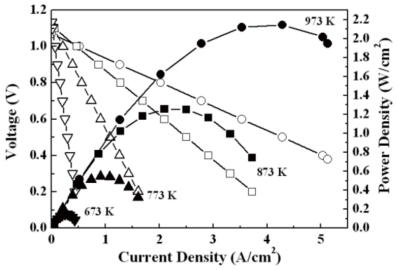

Fig. 1. Power generation property of the cell having SSC-SDC double columnar electrode..

S-P21-G

Effect of the improvement of tolerance factor and the insertion of A-site vacancy on the thermoelectric properties of perovskite-type oxide Ca-Mn-O system

H. Kawakami*, H. Takemoto, M. Saito H. Yamamura and S. Yamaguchi
Department of Material and Life Chemistry, Faculty of Engineering, Kanagawa University, 3-37-1 Rokkakubashi, Kanagawa-ku, Yokohama, 221-8686, Japan *hiroshikawakami627@yahoo.co.jp

Thermoelectric materials are usually evaluated in terms of figure of merit, $Z=S^2\sigma/\kappa$, where S, σ and κ represent the Seebeck coefficient the electrical conductivity and the thermal conductivity, respectively. Perovskite-type oxide systems, $Ca_{1-x}Nd_xMnO_3$, $Ca_{1-x}Nd_{2x/3}\square_{x/3}MnO_3$ and $Ca_{0.865-y}Sr_yNd_{0.09}\square_{0.045}MnO_3$ were synthesized by a standard ceramic technique. The thermoelectric properties were investigated as functions of temperature and composition. Figure 1 show the electrical conductivity of Ca-Mn-O (Nd= 0.09) systems. The electrical conductivities of Ca-Mn-O systems increased in the insertion of A-site vacancy into the $Ca_{1-x}Nd_xMnO_3$ system. In addition, the electrical conductivities of Ca-Mn-O system increased in the substitution of Sr ion on the basis of tolerance factor. Although the electrical conductivity increased due to heightening the crystal symmetry by both a insertion of A-site vacancy into the perovskite-type structure and a improvement of tolerance factor, the Seebeck coefficient of $Ca_{1-x}Nd_{2x/3}\square_{x/3}MnO_3$ and $Ca_{0.865-y}Sr_yNd_{0.09}\square_{0.045}MnO_3$ systems did not change when the both systems have same Nd content, but showed the similar value of $Ca_{1-x}Nd_xMnO_3$ system. The thermal conductivity decreased by a insertion of A-site vacancy into the perovskite-type structure.[1)]

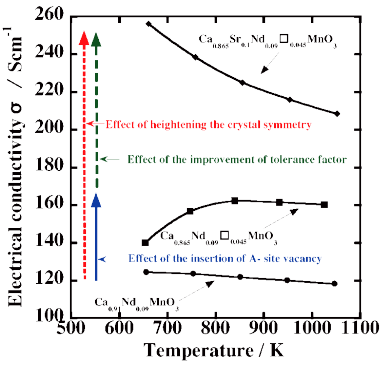

Fig.1 Electrical conductivity for Ca-Mn-O system.

As a result, it can be speculated that the insertion of A- site vacancy into perovskite and the improvement of tolerance factor play an important role in the thermoelectric properties.

1) H. Kawakami, H. Noda, M. Sugimoto, T. Takayama and H. Yamamura, Transactions of the Materials Reseach Society of Japan, 34[2] (2009)

Session T

T-19-M

The Crystal growth of In-Se by Vapor Transport Method

N. Takano[1)*], H. Kohri[2)] and T. Yagasaki[2)]
1)Graduate school, Kogakuin University, 2665-1, Nakano-machi, Hachioji, Tokyo, 192-0015, *bm11033@ns.kogakuin.ac.jp
2)Faculty of Engineering, Kogakuin University, 2665-1, Nakano-machi, Hachioji, Tokyo, 192-0015

Solar cell cannot generate in infrared wavelength region. On the other hand, the thermophotovoltaic (TPV) material can generate with infrared and/or near-infrared rays. Then the development of combined system with solar cell and TPV cell has been attempted. The α and β phase of In_2Se_3 have attracted attention as TPV materials because of the band gap, which is 1.3 eV. The crystal structure of In_2Se_3 is contained the vacancies at one third of the cation sites. It is well known that In_2Se_3 forms a variety of crystal polymorphism because of the vacancy. We investigated about the crystal growth of In_2Se_3 by vapor transport method, using bulk In_2Se_3 as the source material.

The quartz ampoule encapsulated only bulk In_2Se_3 or bulk In_2Se_3 and Si substrate was heated by temperature gradient furnace. The bulk In_2Se_3 was placed at hot side in quartz ampoule and Si substrates were placed at alternative side. The temperature of In_2Se_3 source side was kept at 1050 K, and the alternative side was kept at 850 K. The surface of each sample was observed by SEM. The phase identification of each sample was achieved by XRD.

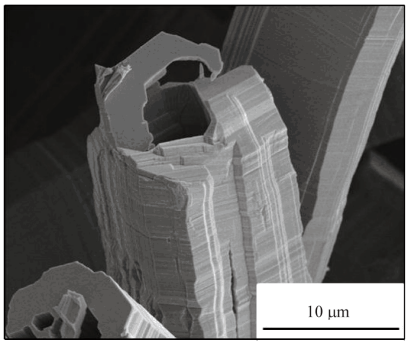

Fig. 1 SEM image of In_2Se_3 hollow hexagonal cylinders.

The hollow hexagonal cylinders with diagonal dimension of approximately 10 μm were observed in the quartz ampoule encapsulated only bulk In_2Se_3. The layers with thickness of 200 nm were stacked in a longitudinal direction of the hollow hexagonal cylinder. From the results of powder XRD analysis, these hollow hexagonal cylinders were contained α, β, γ and δ phase of In_2Se_3. The nanoparticles were observed in the quartz ampoule encapsulated bulk In_2Se_3 and Si substrate. The nanoparticle with diameter of 50 nm sparsely deposited on the substrate surface the textured surface, which was compactly-arranged square pyramid, was observed at the surface of the Si substrate. It seems that these square pyramids were formed by etching and eutectic reaction between Si and deposited In. The details of nanoparticle are now under investigation.

Session U

U-P01-D

Interaction between Peptides and Hypochlorous acid

M. Yasutomi[1)], Y. Sasaki[1)], A. Iwasawa[2)] and Y. Nishimoto*[1)]
[1]Kanagawa Univ., Tsuchiya Hiratsuka Kanagawa 259-1293
[2]Tokyo Institute of Technology, Midori-ku, Yokohama, Kanagawa 226-8502,
*y24moto@kanagawa-u.ac.jp

An electrolyzed strong acid aqueous solution is called "functional water", because of its strong bactericidal activity and effects on viruses. Functional water can be prepared easily in a hospital; it was used in the medical field. Functional water has unique characterization such as a high oxidation-reduction potential, strong acidity and a high concentration of dissolved oxygen (pH2.2 ~ 2.7, ORP 1.3 V ~, available chlorine concentration: 0.28 ~ 0.84 mmol/L). Aqueous solution with the same concentration of the available chlorine as electrolyzed was prepared with NaClO (KClO), HCl and NaCl (KCl). The pH and ORP values and the bactericidal effect of the prepared solution were almost the same as those of the electrolyzed strong acid aqueous solution. From the analytical results, a strong acid aqueous solution can be prepared without electrolysis. Most characteristics of the electrolyzed strong acid aqueous solution were explicable by its components. From these results, bactericidal effects of electrolyzed strong acid aqueous solution were mainly ascribed to HClO which was almost responsible for the available chlorine. The interaction diminished more on the alkaline side, and at pH12, no change in the chemical conformation caused by the interaction was observed. These results show the agreement with the results that the bactericidal effects weaken on the alkali side. In this study, the effect of the peptide on the hypochlorite was examined.

By the use of hypochlorous solution with an adjusted pH, the interaction of glutathione (GSH, Glu-Cys-Gly), Cys-Gly or Ala-Gln and hypochlorous acid was investigated by ^{13}C NMR and Circular dichroism (CD) and Cyclic voltammetry (CV).

References
1) Atsuo IWASAWA, Yoshiko NAKAMURA, Kei IONOUE, Tomokazu NIWA and Yuko NISHIMOTO, *Bokin Bobai*, **32**, 301-306 (2004),
2) Atsuo IWASAWA, Yoshiko NAKAMURA, Tomokazu NIWA and Yuko NISHIMOTO, *Bokin Bobai*, **30**, 635-643 (2002),
3) Yuko NISHIMOTO, Yuko MORISHITA and Mihoko KAITSUKA, *Bunseki Kagaku*, **45**, 701-706 (1996),
4) Atsuo IWASAWA, Aya HARANO, Yuki AKIYAMA, Yoshiko NAKAMURA and Yuko NISHIMOTO, *Bokin Bobai*, **37**, 243-252 (2009),
5) Atsuo IWASAWA, Mao YASUTOMI,Yoshiko NAKAMURA and Yuko NISHIMOTO, *Bokin Bobai*, **38**, 69-74 (2010),
6) Mao YASUTOMI, Atuo IWASAWA and Yuko NISHIMOTO, *Bokin Bobai*, **39** (2011) in press

U-P11-M

Analysis of Adsorption Behavior of Beryllium(II) on Copper-Oxide Colloids in Water

S. Shimada[1)], K. Bessho*[2)], S. Katsuta[1)], H. Monjushiro[2)], Y. Kudo[1)] and Y. Takeda[1)]
[1)] Graduate School of Science, Chiba University, 1-33 Yayoi-cho, Inage, Chiba 263-8522, Japan, [2)] Radiation Science Center, High Energy Accelerator Research Organization (KEK), 1-1 Oho, Tsukuba 305-0801, Japan, *kotaro.bessho@kek.jp

At high-energy accelerator facilities, it is an important subject that copper-oxide (CuO) colloids in cooling water adsorb radionuclides, especially ^{7}Be, and circulate through the cooling water systems. In this study, the adsorption behavior of Be(II) on commercially available CuO nanoparticles in water was investigated quantitatively under various conditions (pH, ion strength, and CuO amount). The distribution ratio, D, is defined as follows:

D = [the amount of Be adsorbed on the CuO nanoparticles (mol g^{-1})] / [the concentration of Be in the aqueous phase (mol dm^{-3})].

An example of the log D versus pH plot is shown in Fig. 1. The log D value increases monotonously with an increase in pH. It was also found that the D value is independent of the ion strength and the amount of nanoparticles. The detailed analysis of the adsorption data indicated that Be(II) is adsorbed by complex formation with the hydroxyl groups on the CuO surface (>S-OH) according to the following equation:

n >S-OH + Be^{2+} ⇔ $(>S\text{-}O)_nBe^{(2-n)+}$ + n H^+ (n = 1 – 4).

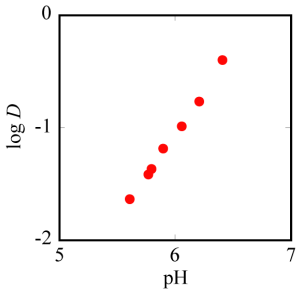

Fig. 1. Distribution ratio of Be(II) as a function of pH.

The surface densities of the hydroxyl groups were evaluated by acid-base titrations. Moreover, the zeta potentials and the particle size distributions of the CuO nanoparticles were measured. The results showed that there is little change in the surface state of the nanoparticles in the pH range where the adsorption experiments were conducted.

Session V

V-10-M

Preparation of Ce^{3+}-doped barium silicon oxynitride by carbothermal reduction / nitridation of spray-pyrolyzed oxide/nitride powder and its luminescence properties

T. Sasaki[1)], H. T. Hintzen[2)], A. C. A. Delsing[2)], H. Kuwahara[3)], S. Koda[1)] and K. Itatani[*1)]
[1)] Department of Materials and Life Sciences, Sophia University, 7-1 Kioi-cho, Chiyoda-ku, Tokyo 102-8554, Japan
[2)] Department of Chemical Engineering and Chemistry, Eindhoven University of Technology, P.O. Box 513, 5600 MB Eindhoven, The Netherlands
[3)] Department of Engineering and Applied Sciences, Sophia University, 7-1 Kioi-cho, Chiyoda-ku, Tokyo 102-8554, Japan
[*]itatani@sophia.ac.jp (Corresponding author)

The conditions for the preparation of regularly-shaped Ce^{3+}-doped oxynitride phosphor powder ($Ba_3Si_6O_9N_4$:Ce^{3+}) were examined by the carbothermal reduction and nitridation (CRN) of oxide/nitride powder prepared by ultrasonic spray pyrolysis (USP). The starting solution with 0.287 mol·dm^{-3} $Ba(NO_3)_2$ and 0.333 mol·dm^{-3} Si_3N_4 was sprayed using an ultrasonic vibrator into the furnace heated at 600ºC in order to obtain the precursor oxide/nitride powder. The resulting powder was composed of the agglomerates with the mean diameter of 0.49 μm, and no crystalline phase was present in the powder. Then the carbon was added to the spray-pyrolyzed powder for carbothermal reduction with the *m* value of 1.5 (*m*: the relative amount of carbon to the stoichiometric amount). The single phase of $Ba_3Si_6O_9N_4$ could be obtained when the mixed powders of oxide/nitride and carbon were nitrided at a temperature as low as 1300ºC in N_2 atmosphere (heating time: 2 h). The mean particle size of the powder prepared by the USP-CRN was 0.31 μm. **Figure 1** shows XRD patterns of the powders obtained by the USP-CRN and by the heating of mixture ($BaCO_3$, Si_3N_4 and SiO_2) at 1350ºC for 2 h in N_2 atmosphere (solid-state reaction: SSR). The crystalline phase was $Ba_3Si_6O_9N_4$ in both cases, and the X-ray intensity of the powder prepared by USP-CRN was comparable to that of the powder prepared by SSR. When the Ce^{3+} was added to the $Ba_3Si_6O_9N_4$, the emission spectra with a peak at 409 nm appeared, showing a blue emission.

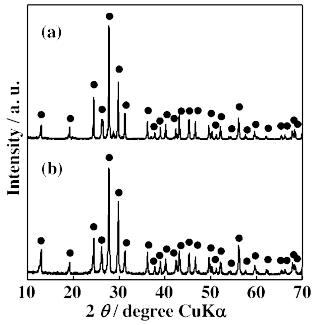

Fig.1. XRD patterns of powders obtained by (a) USP-CRN (heating conditions: 1300ºC, 2 h) and (b) SSR (1350ºC, 2 h) in N_2 atmosphere.
●: $Ba_3Si_6O_9N_4$

V-P21-M

Synthesis of low temperature phase $BiNbO_4$ by flux method.

Y. Maruyama[1)], T. Watanabe[*]
Department of Applied Chemistry, School of Science and Technology, Meiji University, Kanagawa 214-8571, Japan, [1)] Department of Applied Chemistry, School of Science and Technology, Meiji University, Kanagawa 214-8571, Japan, [*]tomowata@ meiji.ac.jp

We succeeded in the synthesis of $BiNbO_4$ by using Bi_2O_3-B_2O_3 eutectic flux. Flux method is a method of crystal growth by cooling flux after solute dissolved in flux melting. The product obtained by Bi_2O_3-B_2O_3 eutectic flux is fine crystal and this method was relatively low temperature reaction than conventional method. The average particle size of $BiNbO_4$ was about 5-10 μm.

Bi_2O_3, Nb_2O_5 and B_2O_3 was mixed at a molar ratio of Bi_2O_3 : Nb_2O_5 : B_2O_3 = 11 : 11 : 9 and put in the alumina boat. The alumina boat was heated at 10 °C/min from room temperature to 800 °C in air. After holding at 800 °C for 10 h, the alumina boat was allowed to naturally cool down to room temperature. The product was separated from the flux by washed with 2 M HNO_3, and finally dried in air at 80 °C.

The obtained product was white colored powder. The X-ray diffraction (XRD) pattern of the product powder is shown in Figure 1. The XRD pattern of the product powder agrees with reported pattern of ICDD data No.01-0820-348. In conclusion, low temperature phase $BiNbO_4$ has been successfully synthesized by flux method at 800 °C for 10 h.

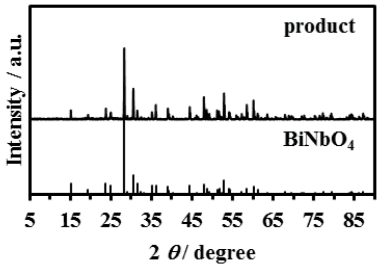

Fig. 1. XRD pattern of product prepared by flux method at 800°C for 10h and standard XRD pattern of ICDD data 01-0820-348.

References : 1) M.A.Subramanian and J.C.Calabrese, *Mat.Res.Bull.*, **28**, 523–529 (1993), 2) Scott S. Dunkle and Kenneth S .Suslick, *J.PHYSICAL CHEMISTRY.*, **113**, 10341–10345 (2009).